Author Manuscript

Author Manuscript

Author Manuscript

Author Manuscript

HHS Public Access

Author manuscript

*Cell Metab*. Author manuscript; available in PMC 2021 November 03.

Published in final edited form as:

*Cell Metab*. 2020 November 03; 32(5): 786–800.e7. doi:10.1016/j.cmet.2020.08.017.

# Insulin and Leptin/Upd2 exert opposing influences on synapse number in fat-sensing neurons

**Ava E. Brent**[1], **Akhila Rajan**[1,2,*]

[1]Basic Sciences Division, Fred Hutch, Seattle, WA 98109.

[2]Lead Contact.

## Summary

Energy sensing neural circuits decide to expend or conserve resources based, in part, on the tonic, steady-state, energy-store information they receive. Tonic signals, in the form of adipose tissue-derived adipokines, set the baseline level of activity in the energy sensing neurons, thereby providing context for interpretation of additional inputs. However, the mechanism by which tonic adipokine information establishes steady-state neuronal function has heretofore been unclear. We show here that under conditions of nutrient surplus, Upd2, a *Drosophila* Leptin ortholog, regulates actin-based synapse reorganization to reduce bouton number in an inhibitory circuit, thus establishing a neural tone that is permissive for Insulin release. Unexpectedly, we found that Insulin feeds back on these same inhibitory neurons to conversely increase bouton number, resulting in maintenance of negative tone. Our results point to a mechanism by which two surplus-sensing hormonal systems, Leptin/Upd2 and Insulin, converge on a neuronal circuit with opposing outcomes to establish energy-store-dependent neuron activity.

## Graphical Abstract

*Correspondence to: akhila@fredhutch.org.

Author Contributions

Conceptualization, A.R.; Methodology, A.R. and A.E.B.; Investigation, A.E.B.; Writing – A.R. and A.E.B.; Funding Acquisition, A.R.

**Publisher's Disclaimer:** This is a PDF file of an unedited manuscript that has been accepted for publication. As a service to our customers we are providing this early version of the manuscript. The manuscript will undergo copyediting, typesetting, and review of the resulting proof before it is published in its final form. Please note that during the production process errors may be discovered which could affect the content, and all legal disclaimers that apply to the journal pertain.

Declaration of Interests

The authors declare no competing interests.

Author Manuscript Author Manuscript Author Manuscript Author Manuscript

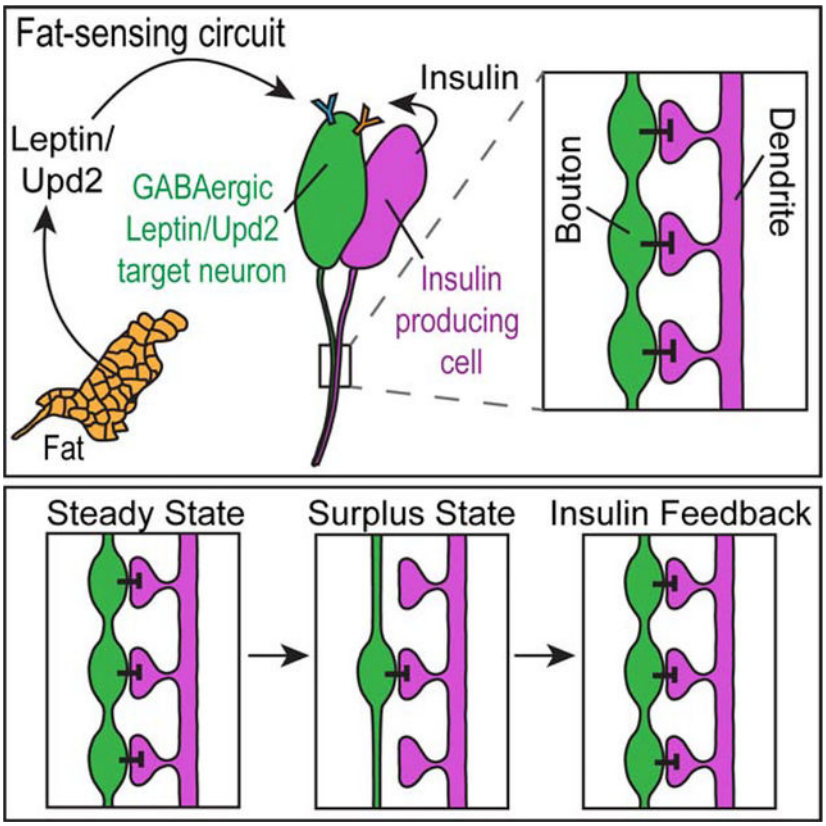


## eTOC

Brent and Rajan show that in response to fat-store levels, leptin/Upd2 modulates synapse number in fat-sensing neurons of Drosophila, ensuring that adipokine responsive neuronal activity reflects fat-store availability. They report an unexpected role for insulin-dependent negative feedback, revealing that fat store maintenance results from opposing actions of leptin/Upd2 and insulin signaling on synaptic structure.

### Keywords

*Drosophila*; JAK/STAT; Upd2; Leptin; Insulin; inhibitory tone; energy homeostasis; Arouser; actin; Gelsolin; Basigin; tonic; phasic

## Introduction

An organism’s ability to sense different nutrient states and respond accordingly is essential to survival: when energy reserves are replete, costly processes like reproduction and immunity can be pursued; under conditions of scarcity, depleted reserves signal metabolic conservation (Flier, 2019). In invertebrates and vertebrates, such homeostatic behavioral decisions are directed by central nervous system (CNS) neurons that receive and interpret systemic, steady-state energy availability information from circulating adipokines such as Leptin (Rajan and Perrimon, 2013; Xu et al., 2018). Derived from adipose tissue and released in proportion to stored fat, Leptin regulates target neuron baseline activity,

Author Manuscript Author Manuscript Author Manuscript Author Manuscript

providing context within which the neurons integrate, interpret, and flexibly respond to additional signals (Timper and Bruning, 2017). The mechanism by which energy store-responsive neurons interact with steady-state information has not heretofore been well understood; yet significantly, dysregulation of the program not only causes energy imbalance, but also underlies serious chronic metabolic disorders such as diabetes and obesity (Flier, 2019). Here we employ a *Drosophila* model of energy surplus-sensing hormones to uncover the mechanism whereby the energy-sensing circuits interpret fat store status to establish baseline activity (Baker and Thummel, 2007; Musselman and Kuhnlein, 2018; Nassel et al., 2013; Rajan and Perrimon, 2011, 2013; Teleman et al., 2012).

In mammals, Leptin works with Insulin to control body weight and energy homeostasis. Circulating levels of both hormones correlate directly with total body fat mass: in conditions of energy depletion, levels decrease; with energy surplus, they increase (Flier, 2019; Timper and Bruning, 2017). Together, Leptin and Insulin inform target neurons on energy stores (Banks, 2004; Flier and Maratos-Flier, 2017). In addition, Insulin release from the pancreatic beta cells regulates carbohydrate and lipid metabolism in peripheral tissues, promoting absorption of nutrients, such as glucose and lipids, as well as storage for later use in the form of glycogen and triacylglycerol (TAG) (Banks, 2004; Flier, 2019; Flier and Maratos-Flier, 2017). However, Leptin and Insulin also fluctuate in a phasic manner during meal intake (Boden et al., 1996; Kolaczynski et al., 1996a; Kolaczynski et al., 1996b; Pinto et al., 2004), making it difficult to detect the mechanism by which tonic as opposed to acute information is communicated to target neurons. Further complicating analysis is the observation that Leptin and Insulin interact with one another, and do so in sometimes synergistic, sometimes antagonistic ways (Flier, 2019). In *Drosophila*, by contrast, the relationship between Leptin and Insulin is better defined (Rajan and Perrimon, 2012).

The fly adipokine JAK/STAT ligand, Unpaired-2 (Upd2), is released by the fat body (FB) adipocytes in proportion to fat stores, and communicates energy availability to the brain (Rajan et al., 2017; Rajan and Perrimon, 2012). Upd2 shares several features with its vertebrate counterpart, Leptin: both measure adiposity, respond to nutritional surplus or scarcity, and undergo restricted secretion during periods of starvation in order to conserve resources. Upd2 regulates how much Insulin is released into circulation from the fly's Insulin-producing cells (IPCs), a group of 14 neuroendocrine cells, homologous to mammalian pancreatic beta cells, that reside in the median neurosecretory cluster of the brain (Geminard et al., 2009; Rajan et al., 2017; Rajan and Perrimon, 2012). *Drosophila* Insulin-like proteins (Dilps) not only regulate nutrient uptake and utilization, but also promote adipocyte cell number as well as FB TAG storage of excess nutrients (DiAngelo and Birnbaum, 2009). In addition, Dilps support many aspects of complex physiology and behavior, such as reproduction, sleep, and immunity (Das and Dobens, 2015; Enell et al., 2010; Lebreton et al., 2017; Nassel et al., 2013; Rulifson et al., 2002). Coordination of energy status with extent of Insulin release thus ensures that the fly's resources are properly distributed.

Upd2 signaling is received not directly by the IPCs, but by a group of proximal neurons that express the Upd2 receptor, Domeless (Dome) (Rajan and Perrimon, 2012). Binding of Upd2 to Dome triggers the STAT signaling pathway such that current nutritional state is reflected

Author Manuscript Author Manuscript Author Manuscript Author Manuscript

(Rajan and Perrimon, 2012). The Upd2-responsive STAT neurons have been shown to be GABAergic (Rajan and Perrimon, 2012); hence, their function in the nutrient-sensing pathway is inhibitory, with Upd2 signaling easing the extent of inhibition in conditions of surplus fat storage. The STAT-expressing neurons thus behave as a rheostat, responding in varying degrees to a tonic signal defined by extent of Upd2 secretion, and thereby imparting appropriate inhibitory tone to the IPCs. This inhibitory, clamp-like control is conserved in vertebrates: Leptin-associated activation of STAT in GABAergic neurons has been shown to underpin Leptin's effect on the hypothalamic circuits (Vong et al., 2011) that inhibit feeding and promote energy expenditure, underscoring that fat store-dependent regulation of inhibitory tone is a conserved property of Upd2/Leptin signaling. Uncovering how Upd2 regulates the extent of inhibitory tone imparted by its target neurons on Insulin release will thus provide insight into how adipokines in general use steady-state fat store information to regulate neural tone.

Here we define the structural organization of the synaptic contact point between the Upd2 target neurons and the IPCs, and develop an assay for steady-state neural activity, using image segmentation-based quantification of axonal boutons. With this assay, we show that Upd2 establishes inhibitory tone by regulating bouton number in its target neurons; that several proteins implicated in reorganization of actin-cytoskeleton organization play a role in the process; and that bouton number is altered to reflect extent of energy stores. Moreover, we found that Insulin itself provides negative feedback to the system by acting on the same synapse to increase bouton number, thereby ensuring that inhibitory tone remains consistent. Hence, the reciprocal effects of Upd2/Leptin and Insulin on bouton number in fat-store sensing neurons establish a feedback loop that is required for proper maintenance and utilization of steady-state fat storage.

## Results

### Characterization of the Upd2-sensing GABAergic STAT neurons

Previous work described a population of STAT-expressing GABA neurons, located in the pars intercerebralis (PI) region of the *Drosophila* brain, that receive fat store information from the FB in the form of the adipokine, Upd2 (Rajan and Perrimon, 2012). While the Upd2-GABA-IPC circuit has been defined, the tools required to manipulate the specific GABAergic STAT neurons in the PI region were lacking. To this end, we screened the InSite collection of Gal4 enhancer trap lines, and identified a Gal4 inserted into the STAT92E gene (Gohl et al., 2011). We examined expression of STAT-Gal4 driven dsRed in the adult brain (Figure 1A), and found STAT activity in several neuron populations, including a set of 6 neurons with somas in the PI region (left panels, yellow arrow), and arborizations in the subesophageal zone (SEZ, yellow bracket). We confirmed that in location and projections, these neurons resembled the Upd2 targets previously described with a STAT-GFP reporter (STAT::GFP) (Rajan and Perrimon, 2012): using STAT-Gal4-driven expression of dsRed, and STAT::GFP; we visualized both populations and found overlapping fluorescence, indicating that both tools capture the same neuron population (Figure S1A). While we also observed STAT neuron populations with somas in the olfactory bulbs (magenta arrow), the SEZ (green arrow) (Figure 1A), and a bilateral dorsal domain (blue arrows), our focus was

Author Manuscript Author Manuscript Author Manuscript Author Manuscript

the STAT-expressing neurons in the brain PI region, hereafter termed the PI-STAT neurons. Co-staining of dsRed with an antibody to Dilp2 revealed that the PI-STAT neuron somas intermingle, but do not overlap, with those of the IPCs (Figure 1A, middle panels): the tracts of both descend together from the PI region to the SEZ (Figure 1A, middle and right panels in, respectively, XY and YZ planes). Note that the yellow signal in the merged images is the result of maximum intensity projections, and does not represent overlapping expression of STAT and Insulin: single XY slices through the PI region exhibit mutually exclusive STAT and IPC somas (Figure S1B).

Previous work demonstrated that the JAK/STAT signaling pathway promotes systemic energy storage (Rajan and Perrimon, 2012). To confirm that our InSite STAT-Gal4 driver included the STAT-expressing neurons that regulate energy storage, we used STAT-Gal4 to induce expression of RNAi transgenes directed against *dome* or *Stat* (Figure 1B). We avoided potential developmental effects arising from interference with JAK/STAT signaling by restricting knockdown to adult STAT-expressing cells, using a tubulin promoter-driven, temperature-sensitive Gal80 ($TubGal80^{ts}$), and shifting to permissive temperature only after eclosion. We verified that knockdown of either *dome* or *Stat* in STAT-expressing cells resulted in decreased systemic TAG storage (Figure 1B), and similarly, that over-expression of either a dominant-negative (DN) or constitutively-active (CA) form of *Stat* resulted in, respectively, decreased or increased TAG storage (Ekas et al., 2010). To target the effects of STAT-Gal4-driven manipulation specifically to STAT-expressing neurons, as opposed to other STAT-expressing cell types, we expressed the temperature-sensitive neuronal activator *TrpA1* (Hodge, 2009) under control of STAT-Gal4. At the permissive temperature, which promotes membrane depolarization, we observed progressive decline of systemic TAG storage over the course of 1 to 3 days (Figure 1C), while at the restrictive temperature, we saw no change in TAG storage (Figure S1C). These observations indicated that the PI-STAT neurons are inhibitory, and that Dome/STAT signaling relieves inhibition to promote accumulation of TAG in the FB.

Insulin release from the IPCs plays an essential role in promoting and regulating systemic fat storage (Das and Dobens, 2015; Rulifson et al., 2002; Zhang et al., 2009): during nutrient-replete conditions, insulin is secreted; upon deprivation, insulin is retained (Geminard et al., 2009; Rajan and Perrimon, 2012). A reliable monitor of insulin release is quantification of one of three *Drosophila* IPC Insulins (Dilp2, 3, and 5) in conjunction with an assay for transcriptional levels (Delanoue et al., 2016; Geminard et al., 2009; Rajan et al., 2017; Rajan and Perrimon, 2012; Zhan et al., 2016). To investigate if the STAT neurons participate in IPC Insulin release, we induced STAT neuron activity for 1 day with TrpA1, and examined Dilp5 expression via immunohistochemistry (IHC). Quantitative immunofluorescence revealed increased Dilp5 protein in the IPCs (Figure 1D)—an outcome indicating either increased Insulin retention or upregulation of Dilp5 transcription. To distinguish these possibilities, we assayed for Dilp 2, 3 and 5 transcript levels in the IPCs following PI-STAT neuron activation for 1 day, and observed that the steady-state mRNA levels of the three IPC-expressed Dilps (Dilp 2, 3 and 5) were not significantly different from control levels (Figure S1D), suggesting that TrpA1-dpendent activation of PI-STAT neurons indeed promotes Insulin retention.

Author Manuscript Author Manuscript Author Manuscript Author Manuscript

Previous work showed that the STAT neurons regulating Insulin release are GABAergic (Rajan and Perrimon, 2012). To verify that our STAT-Gal4 line was regulating Insulin release via a GABAergic population of STAT-expressing cells, we employed the genetic tool Gad1-Gal80, which represses Gal4 activity specifically in GABAergic neurons (Sakai et al., 2009). We combined STAT-Gal4 controlled TrpA1 activation with expression of Gad1-Gal80 to repress TrpA1 activation selectively within GABAergic STAT neurons, and observed that in the presence of Gad1-Gal80, TrpA1 expression in STAT-expressing cells no longer caused Insulin accumulation (Figure 1D), indicating that retention of Insulin in response to TrpA1 expression results from activation specifically in GABA-expressing STAT neurons. To confirm that the PI-STAT-IPC circuit's control of Insulin release is in fact the mechanism by which these neurons regulate systemic fat storage, we sought to demonstrate that activation of Insulin release is sufficient to rescue the physiological effects of PI-STAT neuron TrpA-dependent activation (Figure 1C). Toward this goal, we conducted a 'neuronal epistasis' test between the STAT-expressing neurons and the IPCs, genetically manipulating the neuronal activity of both simultaneously, using a binary-transcriptional expression system [Gal4-UAS (Brand and Perrimon, 1993) and LexA-LexAop (Lai and Lee, 2006)]. We generated flies expressing LexA in the IPCs under control of Dilp2 regulatory elements (Dilp2-LexA) [See methods], and then activated the PI-STAT neurons and IPCs concurrently, via expression of *TrpA1* in both populations. After a shift to permissive temperature for 1 day, we found, as expected, that activation of the STAT neurons reduced TAG storage, while activation of the IPCs increased it. Strikingly, double activation rescued the STAT-driven *TrpA1* phenotype (Figure 1E), indicating that STAT neurons affect systemic TAG levels by way of their regulation of Insulin release. Finally, we confirmed that STAT neuron regulation of fat storage functions downstream of FB-released Upd2 by demonstrating that repression of STAT neuron activity via the potassium channel *Kir2.1* rescued the reduced TAG phenotype previously observed in *upd2* mutant (*upd2Δ*) flies (Rajan and Perrimon, 2012) (Figure 1F).

We next sought to define the point of synaptic contact between the IPCs and the PI-STAT neurons, using the GRASP system (GFP reconstitution across synaptic partners) (Feinberg et al., 2008; Gordon and Scott, 2009). Expressing one half of split-GFP (*spGFP*) in STAT neurons (Figure 2A, first panel), and the other half in the IPCs (Figure 2A, second panel depicts Dilp5 expression), we traced the reconstituted GFP to a contact point between the PI-STAT neurons and IPC tracts, just below the somas in the PI region (Figure 2A, panels 3 and 4, arrows). To visualize the synaptic terminals of the STAT neurons, we expressed a presynaptic marker, GFP-tagged *Synaptotagmin* (*Syt-GFP*), in the neurons (Yoshihara and Littleton, 2002; Zhang et al., 2002), and observed Syt-GFP in a domain running along the IPC tracts, corresponding to the location where GRASP was observed (Figure 2B, arrows). Syt-GFP also marks the PI-STAT processes in the SEZ, as well as the neurons of the olfactory bulb (OB) (Figure 2B). A side view of the Syt-GFP-expressing PI-STAT neurons reveals a contact point with the Dilp-expressing processes that project from the IPC tracts (Figure 2C)—a region previously described as an IPC dendrite domain (Nassel et al., 2013), and corroborated by expression of the dendrite marker DenMark in the IPCs (Figure 2D) (Nicolai et al., 2010). Syt-GFP expression in the PI-STAT neurons was eliminated by Gad1-Gal80, providing additional evidence that these neurons are GABAergic (Figure 2E).

Author Manuscript Author Manuscript Author Manuscript Author Manuscript

In sum, we established a genetic tool, the InSite STAT-Gal4 fly line, for manipulation of Upd2 fat-sensing, GABAergic, STAT neurons in the PI region (PI-STAT neurons); we identified the point of synaptic contact between these neurons and the IPCs; and we demonstrated that since the PI-STAT neurons repress Insulin release to regulate systemic fat storage, they are inhibitory.

## Establishment of presynaptic bouton number as a measure of tonic neuronal activity

Identification of the mechanism by which Upd2-induced STAT signaling disinhibits Insulin release called for development of an assay for PI-STAT neuron activity. We knew that FB-derived Upd2 is a steady-state tonic signal, released in proportion to fat stores and continuously received by the PI-STAT neurons, which in turn use the information to regulate repression of Insulin release in conjunction with fat stores (Rajan and Perrimon, 2012). As we evaluated tools for visualization of tonic activity, we reasoned that changes in baseline tone might present as alterations in the structure of synaptic contacts. Previous studies have shown that the structural organization of boutons--the bud-like presynaptic enlargements located at the ends of axons--can fluctuate in number and/or size in response to varying inputs (Bushey et al., 2011), and that Syt-GFP can be employed to reflect broad synaptic structure (Bushey et al., 2011; Eddison et al., 2011; Schwenkert et al., 2008). Significantly, Syt-GFP has been used to mark bouton number in other homeostatically regulated neurons (Bushey et al., 2011; Eddison et al., 2011). We thus surmised that we could employ Syt-GFP to look for changes in synaptic structure. In the PI-STAT neurons, Syt-GFP labeling is found in regularly spaced structures, likely representing boutons (Figure 3A, rectangle in left panel, middle panel). With this information, we developed an image segmentation protocol to identify each Syt-GFP puncta within a region of interest, defined as the PI-STAT puncta in contact with the Dilp5-labelled IPC tracts (Figure 3A-also see methods). Designation of Syt-GFP puncta in a single brain yielded a value for average puncta number, surface area, and volume (Figure 3B). To verify that an increase in number of synaptic contacts could be visualized as an increase in Syt-GFP puncta, we examined Syt-GFP expression in PI-STAT neurons in which *EndophilinA*, an endocytic gene previously shown to cause synaptic overgrowth (Goel et al., 2019), had been knocked down, and found a corresponding rise in number of Syt-GFP puncta (Figure S2).

To ascertain the suitability of Syt-GFP bouton characteristics—including bouton number, volume, surface area, and organization--as a proxy for tonic neuron activity, we performed image segmentation analysis of adult brain Syt-GFP puncta under two conditions that impair JAK/STAT signaling: knock-down of either *dome* or *Stat*. In both cases, bouton number increased compared to control-RNAi (Figure 3C). Quantification confirmed that reduced JAK/STAT activity in PI-STAT neurons significantly increased bouton number by ~65% [average control-RNAi Syt-GFP bouton number = 48; STAT-RNAi = 79; Dome-RNAi = 77; p-value $p<0.005$ (Figure 3D)]; however, average puncta volume and surface area remained unchanged (Figure 3E–F). To determine if the increase in PI-STAT neuron bouton number following reduced STAT signaling (Figure 3C,D) was a response downstream of STAT signaling, and not the result of a more general neuronal membrane depolarization-dependent mechanism, we examined Syt-GFP puncta number after TrpA1-induced neuron activation for 1 or 2 days. We observed no changes in Syt-GFP-expressing boutons (Figure S2B)--

Author Manuscript Author Manuscript Author Manuscript Author Manuscript

confirming that the bouton number increases we detected were regulated directly by STAT signaling (Figure 3D). Based on our segmentation analysis, we concluded that the Upd2/Dome/STAT pathway governs IPC activity by altering the number of axonal boutons in the PI-STAT neurons, and that quantification of bouton number would provide a read-out of steady-state neuron activity downstream of JAK/STAT signaling.

## A role for *arouser* in the regulation of bouton number in PI-STAT neurons

Having established an assay for evaluating tonic PI-STAT neuron activity, we performed a candidate-based transgenic RNAi screen to identify genes involved in mediating STAT's effect on bouton number, and found potential candidates with upstream STAT binding sites (see methods, Table S1). In several cases, fat storage was decreased, suggesting that these genes are positively regulated in response to Upd2 signaling. Among our candidates, three have been shown to function in other physiological processes—for example, alcohol sensing, learning, and memory--all of which involve regulation of neuronal activity in response to fluctuating internal or external stimuli (Table S2). One such gene, *arouser* (*aru*), regulates ethanol sensitivity via modulation of bouton number (Eddison et al., 2011). Given the parallel importance of bouton number to regulation of the fat-sensing PI-STAT-IPC circuit by JAK/STAT signaling (Figure 3C, D), we wondered if Aru might play a downstream role in the PI-STAT-IPC circuit as well.

We tested *aru*'s role by assessing the effect of *aru* loss on fat storage. We detected reduced systemic TAG storage in three loss-of-function *aru* alleles compared to control flies (Figure 4A), and saw a similar TAG phenotype following expression of either of two independent *aru*-RNAi lines in adult fly STAT-expressing cells (Figure 4B). Moreover, over-expression of a myc-tagged version of *aru* in STAT-expressing cells led to increased TAG storage (Figure 4C). Altogether, our results supported that Aru function in STAT-expressing cells is both necessary and sufficient to regulate systemic TAG storage. Although our RNAi screen identified *aru* as a potential STAT target gene, however, we have not directly demonstrated that STAT binds the *aru* regulatory elements. It thus remains possible that Aru functions either downstream of, or in parallel to STAT signaling. To query the possibility that Aru functions downstream of STAT signaling, we employed a genetic epistasis approach by co-expressing *aru-myc* with *Stat*-RNAi in the PI-STAT neurons of adults, and then measuring TAG levels (Figure 4D). While knock-down of *Stat* alone reduced systemic TAG, simultaneous over-expression of *aru-myc* increased it, similar to the result we obtained when *aru* alone was over-expressed, and consistent with Aru functioning downstream of JAK/STAT signaling in the PI-STAT neurons. To investigate if Aru's effect on TAG storage depends on Aru activity in STAT-expressing neurons, we asked if repression of STAT neuron function in *aru* mutants would rescue TAG storage. Following repression with the modified Shaker K+ channel, EKO (White et al., 2001), we observed restored systemic TAG storage to WT levels (Figure 4E), verifying that Aru indeed functions in STAT-expressing neurons to control fat storage. To determine if Aru acts within PI-STAT neurons to control Insulin release, we looked at expression of Dilp5 protein in IPCs following *aru* knockdown, and noted significant Insulin retention (Figure 4F). Because one *aru* allele, *8–128*, results from insertion of a Gal4-containing P[GawB] element within the *aru* locus (Eddison et al., 2011), we were able to further evaluate a role for Aru-expressing neurons in regulation of Insulin

Author Manuscript Author Manuscript Author Manuscript Author Manuscript

release by demonstrating that expression of dsRed under control of 8–128-Gal4 marks a population of PI neurons that resemble the PI-STAT neurons in location (Figure S3A).

With confirmation of Aru's role in Insulin release and fat storage, we speculated that Aru might be carrying out these functions via regulation of PI-STAT neuron bouton number. Following *aru* knockdown, segmentation analysis of PI-STAT Syt-GFP puncta showed an increase in average bouton number, while over-expression of *aru-myc* showed a decrease (average control Syt-GFP bouton number = 50; aru-RNAi = 78; aru-myc = 34; p-value $p<0.005$; Figure 4G, H). Changes in bouton number may not, however, reflect number of synaptic contacts, since neurons may alter synapse number and/or activity to compensate for bouton number fluctuation (Goel et al., 2019; Gratz et al., 2019; Harris et al., 2018; Huang et al., 2020; Mosca and Luo, 2014). To assess if the bouton number changes we observed corresponded with changes in synapse number and activity, we applied a two-pronged approach: i) we examined expression of Bruchpilot (Brp), a presynaptic marker of active zones and a reflection of synapse number (Huang et al., 2020); and ii) we assayed the expression of a synaptophysin-tagged, pH-sensitive version of red-fluorescent Tomato (Syp-pHTomato), a reporter of activity-dependent exocytosis (Pech et al., 2015). Using Syt-GFP to mark the boutons of PI-STAT neurons, and either control or *aru-myc* over-expression, we measured total fluorescence intensity of an antibody for Brp in the PI-STAT region, and observed that over-expression of *aru-myc* resulted in parallel reductions in bouton and synapse number. (Figure S3B, C). By contrast, analysis of Syp-pHTomato following *aru* knockdown revealed that while total fluorescence intensity of the PI-STAT Syp-pHTomato domain increased--reflecting greater presence of boutons compared to control-RNAi (Figure S3D, E)--the average intensity of Syp-pHTomato fluorescence within the PI-STAT boutons remained similar to that of control-RNAi (Figure S3F). Hence, synapse activity was not altered to compensate for bouton reduction, supporting that PI-STAT bouton/synapse reduction reflects a true decrease in GABA-dependent inhibitory tone.

## Aru works together with Basigin to alter PI-STAT neuron bouton number via regulation of the actin cytoskeleton

To investigate how Aru alters bouton number in the PI-STAT neurons, we employed immunoprecipitation and mass spectrometry (IP-MS) to look for Aru-interacting proteins in *Drosophila* S2R+ cells (see methods). From our Aru IP-MS screen, we selected a set of candidates (Table S3), among them Basigin (Bsg), an immunoglobulin domain-containing transmembrane protein that has been implicated in the regulation of presynaptic cytoskeletal architecture (Besse et al., 2007). Notably, our lab had independently identified *Bsg* in an RNAi screen as a potential STAT-target gene: following knockdown of *Bsg* in STAT-expressing cells, systemic TAG storage was reduced (Figure 5A, Table S2). To ascertain if Bsg, like Aru, impacts PI-STAT neuron bouton number, we performed *Bsg* knockdown in STAT-expressing cells, followed by segmentation analysis on Syt-GFP puncta, and saw an increase in bouton number (average control-RNAi Syt-GFP bouton number = 53; Bsg-RNAi = 67; p-value $p<0.05$; Figure 5B and C).

Bsg has previously been shown to interact with the presynaptic actin cytoskeleton (Besse et al., 2007). As Aru is a member of the Epidermal Growth Factor Receptor Substrate 8 (Eps8)

Author Manuscript Author Manuscript Author Manuscript Author Manuscript

family of proteins that also function to regulate dynamic changes in F-actin organization, we speculated that actin reorganization might underlie the bouton number phenotype we had observed following manipulation of Aru or Bsg. To visualize the presynaptic actin cytoskeleton in the PI-STAT neurons, we examined expression of two genetically-tagged F-actin binding proteins, Moesin-GFP (Edwards et al., 1997) and F-Tractin-tdTomato (Tractin) (Spracklen et al., 2014)--each under control of STAT-Gal4--and found expression of both in the PI-STAT boutons (Figure 5D). Co-expression of Tractin and Syt-GFP showed localization in an overlapping domain (Figure 5D). Following knockdown of aru, *Bsg*, or *Stat*, we employed Moesin-GFP to look for disruptions in the PI-STAT neuron actin cytoskeleton, and detected increased and irregular Moesin-GFP expression in the PI-STAT neurons, while over-expression of *aru-myc* reduced Moesin-GFP expression (Figure 5E; S4). These results point to a mechanism in which Aru and Bsg regulate bouton number by altering presynaptic actin.

Actin plays many roles in neurons, including establishment of presynaptic architecture, regulation of synaptic vesicle release, and construction of new synaptic contacts (Cingolani and Goda, 2008; Nelson et al., 2013). To investigate how Aru and Bsg might alter the actin cytoskeleton to affect PI-STAT neuron activity, we hypothesized that Aru/Bsg-mediated disassembly of actin functions to eliminate presynaptic contacts, thereby reducing inhibition of the IPCs. In support of this possibility, our IP-MS experiment identified the actin-severing protein Gelsolin (Gel) as a potential Aru interactor (Table S3). A key regulator of actin filament assembly and disassembly, Gel binds to the barbed ends of actin filaments and severs them, thereby preventing monomer exchange. Because Gel's actin-severing function has been previously shown to function during synapse elimination (Meng et al., 2015), we considered that knockdown of *Gel* in PI-STAT neurons would produce an increased bouton phenotype, similar to that observed after *aru-* or *Bsg*-RNAi. Following *Gel* knockdown, our segmentation analysis of PI-STAT Syt-GFP puncta indeed revealed a greater average bouton number (average control-RNAi Syt-GFP bouton number = 48; Gel-RNAi = 59; p-value $p<0.05$; Figure 5F and G). To ascertain if *Gel* functions downstream of *aru* in STAT-expressing cells, we measured systemic TAG levels in flies expressing both *aru-myc* and *Gel* knockdown constructs. While *aru-myc* over-expression resulted in increased TAG storage, and *Gel* knockdown in decreased TAG storage, combined expression mimicked the *Gel-RNAi* TAG phenotype (Figure 5H)—suggesting that *Gel* does genetically function downstream of *aru*, and that wild-type Gel is required for *aru* to carry out its bouton-reducing program. Altogether, these results point to a model in which FB-derived Upd2 determines the level of IPC insulin secretion via the activity of an actin-regulating complex of Aru, Bsg, and Gel, which in turn acts to reduce the extent of inhibitory contact between the PI-STAT neurons and the IPCs.

## PI-STAT neuron bouton number responds to changes in nutrition and Insulin signaling

We next inquired if changes in bouton number could be detected in response to nutrition. As Upd2 is secreted by the FB in proportion to fat stores, and increased fat stores yield greater Upd2 secretion, we reasoned that higher levels of circulating Upd2 should reduce PI-STAT bouton number and promote Insulin release. To test the theory that changes in PI-STAT bouton number reflect expanded fat stores, we fed a high sugar diet (HSD) to flies

Author Manuscript Author Manuscript Author Manuscript Author Manuscript

expressing *Syt-GFP*, and analyzed bouton number after 1, 3, or 5 days (Figure 6A). Compared to flies fed normal food (NF), HSD fly TAG stores progressively increased over the course of 5 days (Figure 6B). Moreover, qPCR for *upd2* in the HSD fly FB tissue demonstrated, as expected, that greater fat stores resulted in higher levels of *upd2* transcription (Figure 6C). Segmentation analysis of PI-STAT Syt-GFP puncta in the brains of flies exposed to HSD for 1, 3, or 5 days revealed a dynamic pattern (Figure 6D): after 1 day, average Syt-GFP puncta number resembled that of flies fed NF. By 3 days, average puncta number for the HSD flies was significantly lower; but by 5 days, average Syt-GFP puncta in HSD flies had returned to NF levels (average NF Syt-GFP bouton number = 46; 1d HSD = 44; 3d HSD = 34, $p<0.05$; 5d HSD = 44; Figure 6D). These results suggest that surplus nutrition and fat storage lead to increased levels of circulating Upd2, which in turn reduces the extent of inhibitory tone on the IPCs by decreasing PI-STAT bouton number--after which inhibitory tone is restored. To test our model that bouton reduction will not occur in HSD *upd2* mutants, we assayed Syt-GFP puncta number after 1, 3, or 5 days in HSD *upd2* mutant flies, and found no decrease in bouton number in *upd2* mutant flies after 3 days HSD, confirming that in the absence of circulating Upd2, PI-STAT neurons fail to properly respond to HSD (average NF Syt-GFP bouton number = 45; 1d HSD = 46; 3d HSD = 46; 5d HSD = 47; Figure 6E).

Restoration of inhibitory tone points to a homeostatic feedback mechanism whereby Insulin release is kept under negative control—a mechanism that would be crucial to the fly's ability to rapidly restrict Insulin secretion in conditions of nutrient deprivation. We wondered if Insulin itself might be the source of negative feedback to the PI-STAT neurons. To examine this possibility, we first had to verify that the Insulin signaling pathway is active in the PI-STAT neurons. From the InSite collection (Gohl et al., 2011), we identified two InR-Gal4 lines, InR-Gal4–0726 and InR-Gal4–0488, both expressed in the PI neurons as well as in the IPCs (Figure 7A and data not shown). InR-Gal4–0726 (hereafter InR-Gal4) exhibits relatively restricted dsRed expression in the adult brain, in a locus primarily within the PI region in both Dilp2-expressing and non-expressing cells (Figure 7A, arrows)--indicating that InR-Gal4 captures a subset of InR-expressing cells. By contrast, InR-Gal4–0488 drives broader expression (data not shown). We examined Syt-GFP in the adult brain InR-expressing cells, and found Syt-GFP puncta resembling the PI-STAT boutons in both number and location (Figure 7B, arrow in side view). We next induced Insulin signaling in adult STAT-expressing cells to evaluate the effect on systemic fat storage. In *Drosophila*, Insulin signals though a pathway that is highly conserved with that of vertebrates: in both, Insulin binds to a target cell receptor (InR), thereby activating downstream targets, among them, phosphoinositide 3-kinase (PI3K), which is additionally negatively regulated by PTEN (Das and Dobens, 2015). To induce Insulin signaling in our adult STAT-expressing cells, we drove expression of activated versions of *InR* (*InR-CA*) and *PI3K* (*PI3K-CA*), and performed RNAi for *Pten* (*Pten*-RNAi). In all three manipulations, we noted diminished systemic TAG, underscoring that Insulin signaling functions in STAT-expressing cells to restrict fat storage. To identify expression of InR within the PI-STAT neurons, we made use of an antibody against human phosphorylated InR, and previously shown to cross-react with *Drosophila* InR (Musashe et al., 2016). We distinguished InR expression in the somas of GFP-marked PI-STAT neurons (Figure 7D, arrows), supporting a potential role for Insulin

Author Manuscript Author Manuscript Author Manuscript Author Manuscript

signaling in the restriction of systemic fat storage via regulation of PI-STAT neuron activity. We tested this role by looking at the effect of activated Insulin signaling on PI-STAT neuron bouton number. Following expression of *InR-CA* in STAT-expressing cells, our segmentation analysis verified an increase in average number of PI-STAT Syt-GFP puncta (average control Syt-GFP bouton number = 52; InR-CA = 65; p-value $p<0.05$; Figure 7E and F). Consistent with this observation, activated PI3K has previously been shown to increase synapse number in the *Drosophila* neuromuscular junction (Howlett et al., 2008). Our collective results thus support a model in which Insulin signaling provides negative feedback to the PI-STAT neurons to promote bouton number and inhibitory tone.

## Discussion

### Convergence of two *Drosophila* hormonal systems determines extent of inhibitory tone

Previous work has shown that release of the adipokine Upd2 from the fat body, in proportion to fat stores, regulates secretion of Insulin from the IPCs in the PI region of the *Drosophila* brain (Rajan and Perrimon, 2012). Because first-order Upd2 target neurons are GABAergic, PI-STAT neurons serve as a clamp on Insulin secretion, providing inhibitory tone that is relieved by Upd2 signaling. Hence Upd2, a surplus hormone reflecting fat store availability, controls another surplus hormone, Insulin, that promotes nutrient uptake and utilization, fat storage, and costly energy-expending behaviors, ensuring that energy expenditure reflects energy availability (Figure S5A) (Nassel et al., 2013; Rajan and Perrimon, 2012, 2013). Our current work reveals how Upd2 alters the activity of its target energy-sensing PI-STAT-IPC circuit by modulating synaptic structure, thereby altering the extent of inhibitory tone provided by the PI-STAT neurons to the IPCs (Figure S5A). Employing a model of diet-induced obesity, we show that prolonged exposure to high sugar diet results in Upd2-dependent structural modifications to bouton number in the PI-STAT neurons, and that these changes, which unfold over the course of several days, reflect steady increases in Upd2 expression as fat reserves are built up. Additionally we identify a potential role for reorganization of the actin cytoskeleton in the regulation of bouton number. Our observations support an energy reserve-sensing model in which STAT signaling in the PI-STAT neurons promotes expression of two genes, Aru and Bsg, that together with Gel regulate presynaptic actin assembly, thereby reducing bouton number (Figure S5A). In this model, steady state levels of Upd2 secreted from the FB determine the extent to which this complex is active and, thus, the number of PI-STAT boutons in contact with the IPCs, with the result that inhibitory tone reflects current energy reserves (Figure S5A).

Prolonged surplus nutrition and diminished inhibitory tone on the IPCs could lead to a scenario in which Insulin release is no longer under negative control; however, our finding that bouton reduction in response to surplus is subsequently reversed (Figure 6D) prompted us to search for a negative feedback mechanism that promotes PI-STAT bouton number. We discovered that the Insulin pathway is expressed in the PI-STAT neurons, and that activation of InR by Insulin indeed promotes bouton number (Figure S5A). We propose that this negative feedback mechanism keeps Insulin secretion under negative control, and that Upd2 and Insulin work together in the PI-STAT-IPC circuit to generate an energy-sensing program that steadily maintains the extent of basal inhibitory tone on Insulin release, irrespective of

Author Manuscript Author Manuscript Author Manuscript Author Manuscript

fluctuations in surplus nutrition intake. In this way, the opposing action by Upd2/Leptin and Insulin generates a feedback loop for fat storage maintenance and utilization (Figure S5A). Since high levels of Insulin secretion during a fasting/starved state would threaten survival, this system of dual hormone inhibitory control is essential. Moreover, the reset of inhibitory tone by negative feedback may serve to prevent the peripheral Insulin resistance that can develop from high levels of circulating Insulin.

## Conservation of adipokine-dependent mechanisms for phasic and tonic regulation

While various aspects of energy-sensing differ between invertebrates and vertebrates, the primary physiological roles of Upd2 and Leptin demonstrate convergence. Both are adipokines that provide energy-store information to the CNS circuits regulating energy expenditure and meal intake; and, in conditions of starvation, the circulating levels of both Upd2 and Leptin must be reduced to conserve energy for survival (Ahima et al., 1996; Rajan et al., 2017; Rajan and Perrimon, 2012). Moreover, while vertebrate neuronal circuitry under control of Leptin signaling is more complex than the fly PI-STAT-IPC circuit we have identified, there are informative similarities there as well. Leptin alters the activities of the agouti related peptide (AgRP) and pro-opiomelanocortin (POMC) target neurons, which act respectively to promote and reduce food intake (Timper and Bruning, 2017): Leptin inhibits the AgRP neurons and enhances the POMCs. Several studies suggest that the bulk of Leptin's anti-obesity function is mediated by its direct effect on the GABAergic neurons that synapse on and inhibit the hypothalamic POMC neurons (Vong et al., 2011; Xu et al., 2018). These GABAergic neurons include the AgRPs, which inhibit POMC neuron activity (Xu et al., 2018). Thus, like the IPCs we have described in *Drosophila*, the POMCs are under GABAergic inhibitory tone, and inhibition is relieved by Leptin signaling (Vong et al., 2011).

Most studies of Leptin's effect on mammalian target neurons focus on Leptin's role in altering a neuron's polarization state--hence their intrinsic excitability--via regulation of hyperpolarizing potassium channels (Baver et al., 2014; O'Malley et al., 2005; Spanswick et al., 1997; Yang et al., 2010). It is probable that this modulation of excitability reflects Leptin's additional function as a communicator of phasic signals, which fluctuate with cycles of meal intake and fasting and thus produce only short-term changes in target neuron function. Studies in mice have shown that Leptin likely uses a synaptic contact-dependent mechanism to regulate its target neurons during acute changes over the course of hours (6 hours) (Pinto et al., 2004). But Leptin's chronic, longer-term effects on target neurons rely on as yet unclear mechanisms that regulate basal tone. With our identification of a Upd2-dependent mechanism for regulation of synaptic structure that functions over the course of days (3–5 days) in response to changes in fat reserves, we provide a means to clarify the specific effects of slow changes in tonically released Upd2 on circuit activity. There is evidence in *Drosophila* that phasic and tonic reporting of nutrient flux may be divided between Upd2 and a second Leptin ortholog, Upd1 (Beshel et al., 2017). Unlike Upd2 and Leptin, Upd1 is not expressed in the adipose tissue, but in the brain, where it has been described as a reporter of satiety to the Neuropeptide F (NPF) neurons that sense hunger and promote foraging behaviors and food intake (Beshel et al., 2017). While the peripheral signal activating release of Upd1 has not been identified, loss of the satiety signal leads to

Author Manuscript Author Manuscript Author Manuscript Author Manuscript

over-eating and an obese phenotype. Notably, Drosophila NPF is the equivalent of the mammalian hormone Neuropeptide Y (NPY), produced by the AgRP neurons to promote food intake (Beshel and Zhong, 2013; Wu et al., 2005). These observations open the possibility that post-meal phasic information on energy availability is transmitted through Upd1, and tonic FB energy store availability through Upd2--and that the two converge to affect Insulin release via the PI-STAT neurons or other circuits. The potential allocation of phasic and tonic functions to Upd1 and Upd2 respectively in *Drosophila* could provide a robust system for analysis of how adipokines respond to and interact with acute and chronic energy inputs.

### Body weight set point, alcohol sensitivity, and the physiology of tolerance

In this study, we have identified a mechanism by which Leptin/Upd2 and Insulin work together to ensure that homeostatic levels of energy-sensing neuron activity are sustained. Our model has implications for the “set-point” theory of energy homeostasis, which proposes that despite short-term variability in energy intake and expenditure, homeostatic negative feedback processes, such as the Insulin feedback mechanism we have described, will maintain body weight within a stable range (Chapelot and Charlot, 2019). If set-point is challenged over long periods of chronic surplus nutrition, however, it may shift such that feedback mechanisms maintain energy homeostasis at a higher level, as occurs in obesity. How long-term exposure to surplus nutrition affects the structure of the PI-STAT-IPC circuit will be an informative field for investigation.

The concept that chronic challenges to energy-sensing can alter homeostatic baseline parallels the pattern of resistance observed following chronic consumption of alcohol. In this context, it is noteworthy that Aru’s regulation of synapse number has been shown to affect response to ethanol: *aru* mutants exhibit hypersensitivity, suggesting that Aru functions in the development of tolerance (Eddison et al., 2011). Moreover, increased resistance to the effects of alcohol has been demonstrated to occur via altered neuronal actin dynamics--similar to the regulation of energy-sensing neuronal circuits defined here (Offenhauser et al., 2006; Sordella and Van Aelst, 2006). These parallels pose the possibility that tolerance to continued surplus nutrition (new set point) and to alcohol consumption may develop via the same mechanism.

### Limitations of Study

While the fruit fly provides a powerful model system for understanding the molecular mechanisms underpinning energy homeostasis, the relevance and generalizability of those mechanisms to human disease remains to be demonstrated in a mammalian experimental model.

## RESOURCE AVAILABILITY

### Lead Contact

Requests for further information, reagents, and resources should be directed to and will be fulfilled by the Lead Contact, Akhila Rajan (akhila@fredhutch.org).

Author Manuscript Author Manuscript Author Manuscript Author Manuscript

### Materials Availability

Drosophila strains generated in this study are available from the corresponding author, Akhila Rajan (akhila@fredhutch.org).

### Data and Code Availability

The datasets generated in this study are available from the corresponding author, Akhila Rajan (akhila@fredhutch.org).

## EXPERIMENTAL MODEL AND SUBJECT DETAILS

### Experimental Animals

**Drosophila melanogaster—**All experimental subjects were *Drosophila melanogaster* males, ages 7–15 days post-eclosion. Flies were cultured in a humidified incubator at 25°C with a 12h light-12h dark cycle, and were fed a standard lab diet, containing per liter: 15 g yeast, 8.6 g soy flour, 63 g corn flour, 5g agar, 5g malt, 74 mL corn syrup. High sugar diet consisted of standard lab diet plus 30% additional sucrose by volume. For RNAi experiments with TubGal80$^{ts}$, crosses were maintained at 18°C for 7 days post-eclosion, after which progeny were shifted to 29°C for 5–7 days. For RNAi experiments without TubGal80$^{ts}$, crosses were placed at 29°C until time of analysis. For TrpA1 experiments, crosses were maintained at 18°C until 7 days post-eclosion, after which they were transferred to 27°C for 1–3 days. For EKO and Kir2.1 experiments with TubGal80$^{ts}$, crosses were maintained at 18°C until 7 days post-eclosion, after which they were transferred to 29°C for 3 days.

**Relevant Genotypes in Each Figure Panel—**Figure 1

| | |
|---|---|
| A | ST AT-Gal4>UAS-dsRed |
| B | STAT-Gal4, TubGal80$^{ts}$>UAS-luc-RNAi<br>STAT-Gal4, TubGal80$^{ts}$>UAS-dome-RNAi<br>STAT-Gal4, TubGal80$^{ts}$>UAS-Stat-RNAi<br>STAT-Gal4, TubGal80$^{ts}$>UAS-luc<br>STAT-Gal4, TubGal80$^{ts}$>UAS-StatDNDC (CA)<br>STAT-Gal4, TubGal80$^{ts}$>UAS-StatE711F (DN) |
| C | STAT-Gal4>UAS-luc<br>STAT-Gal4>UAS-TrpA1 |
| D | STAT-Gal4>UAS-luc<br>STAT-Gal4>UAS-TrpA1<br>STAT-Gal4; Gad1-Gal80>UAS-TrpA1 |
| E | STAT-Gal4>UAS-luc; Dilp2-LexA>LexAop-hrp<br>STAT-Gal4>UAS-TrpA1; Dilp2-LexA>LexAop-hrp<br>STAT-Gal4>UAS-luc; Dilp2-LexA>LexAop-TrpA1<br>STAT-Gal4>UAS-TrpA1; Dilp2-LexA>LexAop-TrpA1 |
| F | yw<br>upd2Δ; STAT-Gal4, TubGal80$^{ts}$ >UAS-luc<br>upd2Δ; STAT-Gal4, TubGal80$^{ts}$ >UAS-Kir2.1 |

Figure 2

Author Manuscript Author Manuscript Author Manuscript Author Manuscript

| | |
|---|---|
| A | Dilp2-LexA>LexAop-spGFP11; STAT-Gal4>UAS-spGFP1–10 |
| B, C | STAT-Gal4>UAS-Syt-GFP |
| D | Dilp2-Gal4>UAS-DenMark |
| E | STAT-Gal4>UAS-Syt-GFP<br>STAT-Gal4; Gad1-Gal80>UAS-Syt-GFP |

Figure 3

| | |
|---|---|
| A, B | STAT-Gal4>UAS-Syt-GFP |
| C, D, E, F | STAT-Gal4, TubGal80$^{ts}$>UAS-luc-RNAi, UAS-Syt-GFP<br>STAT-Gal4, TubGal80$^{ts}$>UAS-dome-RNAi, UAS-Syt-GFP<br>STAT-Gal4, TubGal80$^{ts}$>UAS-Stat-RNAi, UAS-Syt-GFP |

Figure 4

| | |
|---|---|
| A | w$^{1118}$<br>aru$^{d08896}$<br>aru$^{8-128}$<br>aru$^{S13}$ |
| B | STAT-Gal4, TubGal80$^{ts}$>UAS-cn-RNAi<br>STAT-Gal4, TubGal80$^{ts}$>UAS-aru-RNAi-#1<br>STAT-Gal4, TubGal80$^{ts}$>UAS-aru-RNAi-#2 |
| C | STAT-Gal4, TubGal80$^{ts}$>UAS-luc<br>STAT-Gal4, TubGal80$^{ts}$>UAS-aru-myc |
| D | STAT-Gal4, TubGal80$^{ts}$>UAS-lacZ, UAS-luc-RNAi<br>STAT-Gal4, TubGal80$^{ts}$>UAS-lacZ, UAS-Stat-RNAi<br>STAT-Gal4, TubGal80$^{ts}$>UAS-aru-myc, UAS-luc-RNAi<br>STAT-Gal4, TubGal80$^{ts}$>UAS-aru-myc, UAS-Stat-RNAi |
| E | w$^{1118}$<br>aru$^{d08896}$; STAT-Gal4, TubGal80$^{ts}$>UAS-luc<br>aru$^{d08896}$; STAT-Gal4, TubGal80$^{ts}$>UAS-Eko |
| F | STAT-Gal4, TubGal80$^{ts}$>UAS-cn-RNAi<br>STAT-Gal4, TubGal80$^{ts}$>UAS-aru-RNAi-#1 |
| G, H | STAT-Gal4, TubGal80$^{ts}$>UAS-cn-RNAi, UAS-Syt-GFP<br>STAT-Gal4, TubGal80$^{ts}$>UAS-aru-RNAi-#1, UAS-Syt-GFP<br>STAT-Gal4, TubGal80$^{ts}$>UAS-aru-myc, UAS-Syt-GFP |

Figure 5

| | |
|---|---|
| A | STAT-Gal4, TubGal80$^{ts}$>UAS-cn-RNAi<br>STAT-Gal4, TubGal80$^{ts}$>UAS-Bsg-RNAi-#1<br>STAT-Gal4, TubGal80$^{ts}$>UAS-Bsg-RNAi-#2 |
| B, C | STAT-Gal4, TubGal80$^{ts}$>UAS-cn-RNAi, UAS-Syt-GFP<br>STAT-Gal4, TubGal80$^{ts}$>UAS-Bsg-RNAi-#1, UAS-Syt-GFP |
| D | STAT-Gal4>UAS-Moesin-GFP<br>STAT-Gal4>UAS-Syt-GFP, UAS-F-Tractin-tdTomato |
| E | STAT-Gal4, TubGal80$^{ts}$>UAS-cn-RNAi, UAS-Moesin-GFP<br>STAT-Gal4, TubGal80$^{ts}$>UAS-aru-RNAi-#1, UAS-Moesin-GFP |

Author Manuscript Author Manuscript Author Manuscript Author Manuscript

| | |
|---|---|
| | STAT-Gal4, TubGal80$^{ts}$>UAS-aru-myc, UAS-Moesin-GFP<br>STAT-Gal4, TubGal80$^{ts}$>UAS-Bsg-RNAi-#1, UAS-Moesin-GFP<br>STAT-Gal4, TubGal80$^{ts}$>UAS-Stat-RNAi, UAS-Moesin-GFP |
| F, G | STAT-Gal4, TubGal80$^{ts}$>UAS-luc-RNAi, UAS-Syt-GFP<br>STAT-Gal4, TubGal80$^{ts}$>UAS-Gel-RNAi, UAS-Syt-GFP |
| H | STAT-Gal4, TubGal80$^{ts}$>UAS-lacZ, UAS-luc-RNAi<br>STAT-Gal4, TubGal80$^{ts}$>UAS-lacZ, UAS-Gel-RNAi<br>STAT-Gal4, TubGal80$^{ts}$>UAS-aru-myc, UAS-luc-RNAi<br>STAT-Gal4, TubGal80$^{ts}$>UAS-aru-myc, UAS-Gel-RNAi |

Figure 6

| | |
|---|---|
| A | N/A |
| B, C, D | STAT-Gal4>UAS-Syt-GFP |
| E | upd2Δ; STAT-Gal4>UAS-Syt-GFP |

Figure 7

| | |
|---|---|
| A | InR-Gal4>UAS-dsRed |
| B | InR-Gal4>UAS-Syt-GFP |
| C | STAT-Gal4, TubGal80$^{ts}$>UAS-luc-RNAi<br>STAT-Gal4, TubGal80$^{ts}$>UAS-Pten-RNAi<br>STAT-Gal4, TubGal80$^{ts}$>UAS-luc<br>STAT-Gal4, TubGal80$^{ts}$>UAS-InR.del (CA)<br>STAT-Gal4, TubGal80$^{ts}$>UAS-Pi3K92E.CAAX (CA) |
| D | STAT-Gal4>UAS-td-GFP |
| E, F | STAT-Gal4, TubGal80$^{ts}$>UAS-luc, UAS-Syt-GFP<br>STAT-Gal4, TubGal80$^{ts}$>UAS-InR.del (CA), UAS-Syt-GFP |

Figure S1

| | |
|---|---|
| A | STAT::GFP; STAT-Gal4>UAS-dsRed |
| B | ST AT-Gal4>UAS-dsRed |
| C, D | STAT-Gal4>UAS-luc<br>STAT-Gal4>UAS-TrpA1 |

Figure S2

| | |
|---|---|
| A | STAT-Gal4>UAS-luc-RNAi, UAS-Syt-GFP<br>STAT-Gal4>UAS-EndoA-RNAi, UAS-Syt-GFP |
| B | STAT-Gal4>UAS-luc; UAS-Syt-GFP<br>STAT-Gal4>UAS-TrpA1; UAS-Syt-GFP |

Figure S3

Author Manuscript Author Manuscript Author Manuscript Author Manuscript

| | |
|---|---|
| A | $aru^{8-128}$-Gal4>UAS-dsRed |
| B, C | STAT-Gal4, $TubGal80^{ts}$>UAS-luc, UAS-Syt-GFP<br>STAT-Gal4, $TubGal80^{ts}$>UAS-aru-myc, UAS-Syt-GFP |
| D, E, F | STAT-Gal4, $TubGal80^{ts}$>UAS-cn-RNAi, UAS-Syp-pH<br>STAT-Gal4, $TubGal80^{ts}$>UAS-aru-RNAi-#1, UAS-Syp-pH |

Figure S4

| | |
|---|---|
| A | STAT-Gal4, $TubGal80^{ts}$>UAS-cn-RNAi, UAS-Moesin-GFP<br>STAT-Gal4, $TubGal80^{ts}$>UAS-aru-RNAi-#1, UAS-Moesin-GFP<br>STAT-Gal4, $TubGal80^{ts}$>UAS-aru-myc, UAS-Moesin-GFP<br>STAT-Gal4, $TubGal80^{ts}$>UAS-Bsg-RNAi-#1, UAS-Moesin-GFP<br>STAT-Gal4, $TubGal80^{ts}$>UAS-Stat-RNAi, UAS-Moesin-GFP |

Figure S5

| | |
|---|---|
| A | N/A |

## METHOD DETAILS

### RNAi Screen for STAT Target Genes

Candidate STAT targets were identified from the modENCODE consortium's chromatin immuno-precipitation (ChIP) dataset, generated from a well-characterized STAT antibody in *Drosophila* embryos (Celniker et al., 2009). Hits with STAT binding site within 500bp of the transcriptional start were selected, and those showing expression in the adult brain on FlyAtlas database (Chintapalli et al., 2007), and for which multiple independent RNAi lines are publicly available, were designated for further investigation. With these criteria, 35 genes (Table S1) were tested via knock-down in the STAT neurons of adult flies, followed by screening for effects on systemic fat storage by TAG assay, to determine which of the 35 might function in the PI-STAT neuron-IPC circuit. Ten lines manifested robust fat level changes when their activity was reduced in the STAT-expressing cells (Table S2). To ensure that effects on fat storage were not due to fat tissue activity, each candidate was additionally knocked down within the adipocytes, using the FB-specific driver, Lpp-Gal4 (Brankatschk and Eaton, 2010).

### Cloning and Transgenic Flies

All cloning was performed with Gateway® Technology. *arouser* cDNA cloned into the entry vector (pDONR223-FlyBiORFeome-GE009432) was obtained from the FlyBiORFeome collection maintained at the *Drosophila* Genomics Resource Center (DGRC). LR clonase reaction (Gateway® LR Clonase® II Enzyme mix, Cat#11791–020, Invitrogen) was utilized to move entry vectors into destination vectors compatible with fly transformation, protein production, or cell culture, and with the appropriate N-terminal tags. For Dilp2-LexA, primers 5' – CACCGCGTGCAACTCGACAATC −3' and 5' –

Author Manuscript Author Manuscript Author Manuscript Author Manuscript

AGGTTGCTTTACGATCAAATG - 3' were employed to amplify region upstream of Dilp2, flanking sequences GCGTGCAACTCGACAATC and AGGTTGCTTTACGATCAAATG. 2047bp PCR product was obtained, cloned into pENTRD/TOPO, and transferred, via gateway cloning, to vector pBPnlsLexA-GADflUw-DEST to generate the Dilp2-LexA flies. Dilp-LexA was verified by crossing to LexAop-GFP reporter, and by IHC for Dilp5 and Dilp2. Transgenic fly lines provided by Rainbow Transgenic Flies, Inc.

## Generation of Insulin Antibodies

Anti-Dilp5 and chicken anti-Dilp2 primary antibodies were developed by New England Peptide (NEP). Peptide $H_2$N-CPNGFNSMFA-OH was injected into rabbits for Dilp5, and Ac-CEEYNPVIPH-OH into chickens for Dilp2.

## Immunoprecipitation and Mass Spectrometry

For Immunoprecipitation (IP) from S2R+ cells: Protein for experimental and control conditions was prepared by lysing 2 wells of a 6-well dish, 4 days post-transfection. Cells were extracted by incubation in lysis buffer (10 mM Tris–HCl [pH 7.5], 150 mM NaCl, 0.5 mM EDTA, 0.5% [v/v] NP-40, 1 mM PMSF, 1× complete protease inhibitor cocktail [Roche]) for 30 min on ice. Extract was cleared by centrifuge at 20,000 × g for 10 min at 4°. Myc was immunoprecipitated using a camelid Myc-Trap™ Magnetic Agarose (cat# ytma-10, Chromotek) antibody, per manufacturer's protocol. Immunoprecipitates were electrophoresed approximately 1 to 2 centimeters into a SDS-PAGE gel. Stained gel band was cut out and proteolytically digested with trypsin as described (Cheung et al., 2017). Desalted peptides underwent LC-MS/MS with an OrbiTrap Elite mass spectrometer. Collected data analyzed by Proteome Discoverer v2.2. Identified peptides filtered to 1% FDR.

## Triglyceride Measurements

TAG assays were carried out as previously described (Rajan et al., 2017). In brief: Flies were homogenized in PBST (PBS + 0.1% Triton X-100) using 1mm zirconium beads (Cat#ZROB10, Next Advance) in a Bullet Blender® Tissue homogenizer (Model BBX24, Next Advance). Samples were heated to 70°C for 10 minutes, then centrifuged at 14,000 rpm (in refrigerated tabletop centrifuge). 10.0 μl of the supernatant was applied to determine level of TAG in sample, using the following reagents obtained from Sigma: Free glycerol (cat # F6428–40ML), Triglyceride reagent (cat# T2449–10ML), and Glycerol standard (cat# G7793–5ML).Three adult males employed per biological replicate. Note: For adult TAG assays, the most consistent results, with lowest standard deviations, were obtained with 10 day old males. TAG readings from whole fly lysate (n=4 replicates of 3 flies each) were normalized to number of flies per experiment. Normalized ratio from the control served as baseline, and data is represented as fold change of experimental genotypes with respect to the control. Statistical significance quantified by 2-tailed t-test on 3–6 biological replicates per condition. Error bars indicate %SD (Standard Deviation).

Author Manuscript Author Manuscript Author Manuscript Author Manuscript

### qPCR for *upd2* and *Dilps*

qPCR Total RNA prepared from 12–15 fat bodies per genotype, using the Direct-zol RNA miniprep kit (Zymo Research, cat#R2071). cDNA prepared with iScript cDNA Synthesis (Bio-Rad, cat#1708891), and 1 mg RNA applied per reaction. qPCR performed with iQ SYBR Green Supermix (Bio-Rad, cat#1708882). *rpl13A* and *robl* employed to normalize RNA levels. Relative quantification of mRNA levels calculated with comparative CT method. Primers used in this study can be found in Table S4.

### Immunostaining, Confocal Imaging, and Analysis

Immunostaining of adult brains was performed as previously described (Rajan et al., 2017). In brief: Adult brains were dissected in PBS, then fixed overnight in cold 0.8% Para-formaldehyde (PFA) in PBS at 4°C. The following day, tissues were washed multiple times in 0.5% BSA and 0.5% Triton X-100 in PBS (PAT). Tissues were pre-blocked in PAT+ 5% NDS for 2 hours at RT, then incubated overnight with primary antibody at 4°C. The following day, tissues were washed multiple times in PAT, re-blocked for 30 minutes in PAT + 5% NDS, then incubated in secondary antibody in block (final concentration of 1:500) for 4 hours at RT. Samples were washed 3X-5X, 15 minutes per wash, in PAT, then mounted on slides with one layer of Scotch Tape spacers in Slowfade gold antifade. For detection of InR, adult brains were incubated in primary antibody for 2 days at 4°C. Primary antibodies: chicken anti-Dilp2 (1:250; this study); rabbit anti-Dilp5 (1:500; this study); mouse anti-GFP (1:100; Sigma, cat# G6539); chicken anti-GFP (1:2000; Abcam cat#ab13970); rabbit anti-RFP (1:500; Rockland cat#600-401-379); and rabbit anti-phospho-InR β (Tyr1146) (1:1000; Cell Signaling cat#3021); anti-Brp (1:200; DSHB NC82). Secondary antibodies: goat anti-rabbit Alexa 568 (1:500; Thermo Fisher Scientific cat#A11036); donkey anti-chicken Alexa 488 (1:500; Jackson ImmunoResearch cat#703-545-155); donkey anti-mouse Alexa 488 (1:500; Jackson ImmunoResearch cat#715-545-150); and donkey anti-chicken Alexa 647 (1:500; Jackson ImmunoResearch cat#703-605-155). Images captured with Zeiss LSM 800 confocal system, and analyzed with Zeiss ZenLite, ImageJ, and AIVIA (DRVISION Technologies). To measure intensity of Dilp expression, ImageJ-calculated mean gray values were averaged from maximum intensity projections (MIPs) of a similar number of confocal stacks. Average values were normalized to control. To measure total fluorescence intensity of Brp, Moesin-GFP, or Syp-pHTomato expression, ImageJ-calculated integrated density values were collected for either XY slices (Brp) or MIPs (Moesin-GFP, Syp-pHTomato) of PI-STAT neurons in a fixed size ROI in adult brains. Average values were normalized to control.

### Puncta Segmentation and Analysis

Using DRVISION's AIVIA software, we developed an in-house 3D recipe to detect and segment Syt-GFP puncta. The recipe was calibrated on STAT-Gal4>UAS-Syt-GFP-expressing adult brains. To analyze PI-STAT Syt-GFP puncta, Syt-GFP-expressing brains were co-stained with antibody to Dilp5, and region of interest at contact point between PI-STAT neurons and IPCs selected from 3D projections. The segmentation recipe was run, and any Syt-GFP expression not in contact with the Dilp5-expressing processes was manually eliminated. Software determined number, surface area, and volume of the segmented objects

Author Manuscript Author Manuscript Author Manuscript Author Manuscript

(Syt-GFP puncta). Average values were calculated for each brain, and datasets interpreted in GraphPad. Statistical significance quantified by 2-tailed t-test or 1-way ANOVA on 10–28 adult brains. Error bars represent SEM. To assess intensity of Syp-pHTomato expression in individual boutons, Syp-pH puncta were identified as described for Syt-GFP puncta.

## QUANTIFICATION AND STATISTICAL ANALYSIS

Image analysis was carried out in ImageJ, ZenLite, and AIVIA. Details can be found in Method Details, Figure Legends, and Results. Excel or Graph Pad Prism 7 software was used for data quantification and generation of graphs. T-test was employed to compare data within two groups. One-way ANOVA followed by Turkey's multiple comparisons test was employed for comparisons between 3 or more groups. Error bars represent either percent standard deviation (%SD), or standard error of the mean (SEM), as indicated in Figure Legends and Results. Value of n indicated in Figure Legends. We determined that our data-points were normally distributed, based on two measures: i) A Graphpad outlier test did not identify any outliers in our data; and ii) the majority of our data points for a particular condition were relatively similar to one other, with only a small standard error of mean or standard deviation.

## Supplementary Material

Refer to Web version on PubMed Central for supplementary material.

## Acknowledgments

We are grateful to Erika Bach, Benjamin White, Toshi Kitamoto, Kristin Scott, Ulrike Heberlein, Barret D. Pfeiffer and Richard Baines for reagents; Mary Logan for advice on InR IHC; and Laura Holderbaum and Zach Goldberg for technical assistance. Mass spectrometry and analysis were performed by Phil Gafken in the FHCRC Proteomics Core, funded by an NIH Cancer Center Support Grant, P30 CA015704. This study employed Genomic reagents from the DGRC, funded by NIH grant 2P40OD010949, and stocks from the Bloomington Drosophila Stock Center (NIH P40OD018537), Transgenic RNAi Resource project (NIGMS R01 GM084947, and NIGMS P41 GM132087). We thank Pin-Joe Ko for running the RNAi screen funded by the HHMI-EXORP. Our investigation was made possible by grants awarded to AR from NIDDK (R00DK101605), NIGMS (R35GM124593), the Hearst Foundation and Fred Hutch New Development funds.

## References

Ahima RS, Prabakaran D, Mantzoros C, Qu D, Lowell B, Maratos-Flier E, and Flier JS (1996). Role of leptin in the neuroendocrine response to fasting. Nature 382, 250–252. [PubMed: 8717038]

Baker KD, and Thummel CS (2007). Diabetic larvae and obese flies-emerging studies of metabolism in Drosophila. Cell Metab 6, 257–266. [PubMed: 17908555]

Banks WA (2004). The many lives of leptin. Peptides 25, 331–338. [PubMed: 15134858]

Baver SB, Hope K, Guyot S, Bjorbaek C, Kaczorowski C, and O'Connell KM (2014). Leptin modulates the intrinsic excitability of AgRP/NPY neurons in the arcuate nucleus of the hypothalamus. J Neurosci 34, 5486–5496. [PubMed: 24741039]

Beshel J, Dubnau J, and Zhong Y (2017). A Leptin Analog Locally Produced in the Brain Acts via a Conserved Neural Circuit to Modulate Obesity-Linked Behaviors in Drosophila. Cell Metab 25, 208–217. [PubMed: 28076762]

Beshel J, and Zhong Y (2013). Graded encoding of food odor value in the Drosophila brain. J Neurosci 33, 15693–15704. [PubMed: 24089477]

Author Manuscript Author Manuscript Author Manuscript Author Manuscript

Besse F, Mertel S, Kittel RJ, Wichmann C, Rasse TM, Sigrist SJ, and Ephrussi A (2007). The Ig cell adhesion molecule Basigin controls compartmentalization and vesicle release at Drosophila melanogaster synapses. J Cell Biol 177, 843–855. [PubMed: 17548512]

Boden G, Chen X, Mozzoli M, and Ryan I (1996). Effect of fasting on serum leptin in normal human subjects. J Clin Endocrinol Metab 81, 3419–3423. [PubMed: 8784108]

Brand AH, and Perrimon N (1993). Targeted gene expression as a means of altering cell fates and generating dominant phenotypes. Development 118, 401–415. [PubMed: 8223268]

Brankatschk M, and Eaton S (2010). Lipoprotein particles cross the blood-brain barrier in Drosophila. J Neurosci 30, 10441–10447. [PubMed: 20685986]

Bushey D, Tononi G, and Cirelli C (2011). Sleep and synaptic homeostasis: structural evidence in Drosophila. Science 332, 1576–1581. [PubMed: 21700878]

Celniker SE, Dillon LA, Gerstein MB, Gunsalus KC, Henikoff S, Karpen GH, Kellis M, Lai EC, Lieb JD, MacAlpine DM, et al. (2009). Unlocking the secrets of the genome. Nature 459, 927–930. [PubMed: 19536255]

Chapelot D, and Charlot K (2019). Physiology of energy homeostasis: Models, actors, challenges and the glucoadipostatic loop. Metabolism 92, 11–25. [PubMed: 30500561]

Cheung RS, Castella M, Abeyta A, Gafken PR, Tucker N, and Taniguchi T (2017). Ubiquitination-Linked Phosphorylation of the FANCI S/TQ Cluster Contributes to Activation of the Fanconi Anemia I/D2 Complex. Cell Rep 19, 2432–2440. [PubMed: 28636932]

Chintapalli VR, Wang J, and Dow JA (2007). Using FlyAtlas to identify better Drosophila melanogaster models of human disease. Nat Genet 39, 715–720. [PubMed: 17534367]

Cingolani LA, and Goda Y (2008). Actin in action: the interplay between the actin cytoskeleton and synaptic efficacy. Nat Rev Neurosci 9, 344–356. [PubMed: 18425089]

Das R, and Dobens LL (2015). Conservation of gene and tissue networks regulating insulin signalling in flies and vertebrates. Biochem Soc Trans 43, 1057–1062. [PubMed: 26517923]

Delanoue R, Meschi E, Agrawal N, Mauri A, Tsatskis Y, McNeill H, and Leopold P (2016). Drosophila insulin release is triggered by adipose Stunted ligand to brain Methuselah receptor. Science 353, 1553–1556. [PubMed: 27708106]

DiAngelo JR, and Birnbaum MJ (2009). Regulation of fat cell mass by insulin in Drosophila melanogaster. Mol Cell Biol 29, 6341–6352. [PubMed: 19822665]

Eddison M, Guarnieri DJ, Cheng L, Liu CH, Moffat KG, Davis G, and Heberlein U (2011). arouser reveals a role for synapse number in the regulation of ethanol sensitivity. Neuron 70, 979–990. [PubMed: 21658589]

Edwards KA, Demsky M, Montague RA, Weymouth N, and Kiehart DP (1997). GFP-moesin illuminates actin cytoskeleton dynamics in living tissue and demonstrates cell shape changes during morphogenesis in Drosophila. Dev Biol 191, 103–117. [PubMed: 9356175]

Ekas LA, Cardozo TJ, Flaherty MS, McMillan EA, Gonsalves FC, and Bach EA (2010). Characterization of a dominant-active STAT that promotes tumorigenesis in Drosophila. Dev Biol 344, 621–636. [PubMed: 20501334]

Enell LE, Kapan N, Soderberg JA, Kahsai L, and Nassel DR (2010). Insulin signaling, lifespan and stress resistance are modulated by metabotropic GABA receptors on insulin producing cells in the brain of Drosophila. PLoS One 5, e15780. [PubMed: 21209905]

Feinberg EH, Vanhoven MK, Bendesky A, Wang G, Fetter RD, Shen K, and Bargmann CI (2008). GFP Reconstitution Across Synaptic Partners (GRASP) defines cell contacts and synapses in living nervous systems. Neuron 57, 353–363. [PubMed: 18255029]

Flier JS (2019). Starvation in the Midst of Plenty: Reflections on the History and Biology of Insulin and Leptin. Endocr Rev 40, 1–16. [PubMed: 30357355]

Flier JS, and Maratos-Flier E (2017). Leptin's Physiologic Role: Does the Emperor of Energy Balance Have No Clothes? Cell Metab 26, 24–26. [PubMed: 28648981]

Geminard C, Rulifson EJ, and Leopold P (2009). Remote control of insulin secretion by fat cells in Drosophila. Cell Metab 10, 199–207. [PubMed: 19723496]

Goel P, Dufour Bergeron D, Bohme MA, Nunnelly L, Lehmann M, Buser C, Walter AM, Sigrist SJ, and Dickman D (2019). Homeostatic scaling of active zone scaffolds maintains global synaptic strength. J Cell Biol 218, 1706–1724. [PubMed: 30914419]

Author Manuscript Author Manuscript Author Manuscript Author Manuscript

Gohl DM, Silies MA, Gao XJ, Bhalerao S, Luongo FJ, Lin CC, Potter CJ, and Clandinin TR (2011). A versatile in vivo system for directed dissection of gene expression patterns. Nat Methods 8, 231–237. [PubMed: 21473015]

Gordon MD, and Scott K (2009). Motor control in a Drosophila taste circuit. Neuron 61, 373–384. [PubMed: 19217375]

Gratz SJ, Goel P, Bruckner JJ, Hernandez RX, Khateeb K, Macleod GT, Dickman D, and O'Connor-Giles KM (2019). Endogenous Tagging Reveals Differential Regulation of Ca(2+) Channels at Single Active Zones during Presynaptic Homeostatic Potentiation and Depression. J Neurosci 39, 2416–2429. [PubMed: 30692227]

Harris KP, Littleton JT, and Stewart BA (2018). Postsynaptic Syntaxin 4 negatively regulates the efficiency of neurotransmitter release. J Neurogenet 32, 221–229. [PubMed: 30175640]

Hodge JJ (2009). Ion channels to inactivate neurons in Drosophila. Front Mol Neurosci 2, 13. [PubMed: 19750193]

Howlett E, Lin CC, Lavery W, and Stern M (2008). A PI3-kinase-mediated negative feedback regulates neuronal excitability. PLoS Genet 4, e1000277. [PubMed: 19043547]

Huang S, Piao C, Beuschel CB, Gotz T, and Sigrist SJ (2020). Presynaptic Active Zone Plasticity Encodes Sleep Need in Drosophila. Curr Biol 30, 1077–1091 e1075. [PubMed: 32142702]

Kolaczynski JW, Considine RV, Ohannesian J, Marco C, Opentanova I, Nyce MR, Myint M, and Caro JF (1996a). Responses of leptin to short-term fasting and refeeding in humans: a link with ketogenesis but not ketones themselves. Diabetes 45, 1511–1515. [PubMed: 8866554]

Kolaczynski JW, Ohannesian JP, Considine RV, Marco CC, and Caro JF (1996b). Response of leptin to short-term and prolonged overfeeding in humans. J Clin Endocrinol Metab 81, 4162–4165. [PubMed: 8923877]

Lai SL, and Lee T (2006). Genetic mosaic with dual binary transcriptional systems in Drosophila. Nat Neurosci 9, 703–709. [PubMed: 16582903]

Lebreton S, Carlsson MA, and Witzgall P (2017). Insulin Signaling in the Peripheral and Central Nervous System Regulates Female Sexual Receptivity during Starvation in Drosophila. Front Physiol 8, 685. [PubMed: 28943854]

Meng L, Mulcahy B, Cook SJ, Neubauer M, Wan A, Jin Y, and Yan D (2015). The Cell Death Pathway Regulates Synapse Elimination through Cleavage of Gelsolin in Caenorhabditis elegans Neurons. Cell Rep 11, 1737–1748. [PubMed: 26074078]

Mosca TJ, and Luo L (2014). Synaptic organization of the Drosophila antennal lobe and its regulation by the Teneurins. Elife 3, e03726. [PubMed: 25310239]

Musashe DT, Purice MD, Speese SD, Doherty J, and Logan MA (2016). Insulin-like Signaling Promotes Glial Phagocytic Clearance of Degenerating Axons through Regulation of Draper. Cell Rep 16, 1838–1850. [PubMed: 27498858]

Musselman LP, and Kuhnlein RP (2018). Drosophila as a model to study obesity and metabolic disease. J Exp Biol 221.

Nassel DR, Kubrak OI, Liu Y, Luo J, and Lushchak OV (2013). Factors that regulate insulin producing cells and their output in Drosophila. Front Physiol 4, 252. [PubMed: 24062693]

Nelson JC, Stavoe AK, and Colon-Ramos DA (2013). The actin cytoskeleton in presynaptic assembly. Cell Adh Migr 7, 379–387. [PubMed: 23628914]

Nicolai LJ, Ramaekers A, Raemaekers T, Drozdzecki A, Mauss AS, Yan J, Landgraf M, Annaert W, and Hassan BA (2010). Genetically encoded dendritic marker sheds light on neuronal connectivity in Drosophila. Proc Natl Acad Sci U S A 107, 20553–20558. [PubMed: 21059961]

O'Malley D, Irving AJ, and Harvey J (2005). Leptin-induced dynamic alterations in the actin cytoskeleton mediate the activation and synaptic clustering of BK channels. FASEB J 19, 1917–1919. [PubMed: 16166199]

Offenhauser N, Castelletti D, Mapelli L, Soppo BE, Regondi MC, Rossi P, D'Angelo E, Frassoni C, Amadeo A, Tocchetti A, et al. (2006). Increased ethanol resistance and consumption in Eps8 knockout mice correlates with altered actin dynamics. Cell 127, 213–226. [PubMed: 17018287]

Pech U, Revelo NH, Seitz KJ, Rizzoli SO, and Fiala A (2015). Optical Dissection of Experience-Dependent Pre- and Postsynaptic Plasticity in the Drosophila Brain. Cell Rep 10, 2083–2095. [PubMed: 25818295]

Author Manuscript Author Manuscript Author Manuscript Author Manuscript

Pinto S, Roseberry AG, Liu H, Diano S, Shanabrough M, Cai X, Friedman JM, and Horvath TL (2004). Rapid rewiring of arcuate nucleus feeding circuits by leptin. Science 304, 110–115. [PubMed: 15064421]

Rajan A, Housden BE, Wirtz-Peitz F, Holderbaum L, and Perrimon N (2017). A Mechanism Coupling Systemic Energy Sensing to Adipokine Secretion. Dev Cell 43, 83–98 e86. [PubMed: 29017032]

Rajan A, and Perrimon N (2011). Drosophila as a model for interorgan communication: lessons from studies on energy homeostasis. Dev Cell 21, 29–31. [PubMed: 21763605]

Rajan A, and Perrimon N (2012). Drosophila cytokine unpaired 2 regulates physiological homeostasis by remotely controlling insulin secretion. Cell 151, 123–137. [PubMed: 23021220]

Rajan A, and Perrimon N (2013). Of flies and men: insights on organismal metabolism from fruit flies. BMC Biol 11, 38. [PubMed: 23587196]

Rulifson EJ, Kim SK, and Nusse R (2002). Ablation of insulin-producing neurons in flies: growth and diabetic phenotypes. Science 296, 1118–1120. [PubMed: 12004130]

Sakai T, Kasuya J, Kitamoto T, and Aigaki T (2009). The Drosophila TRPA channel, Painless, regulates sexual receptivity in virgin females. Genes Brain Behav 8, 546–557. [PubMed: 19531155]

Schwenkert I, Eltrop R, Funk N, Steinert JR, Schuster CM, and Scholz H (2008). The hangover gene negatively regulates bouton addition at the Drosophila neuromuscular junction. Mech Dev 125, 700–711. [PubMed: 18524547]

Sordella R, and Van Aelst L (2006). Driving actin dynamics under the influence of alcohol. Cell 127, 37–39. [PubMed: 17018272]

Spanswick D, Smith MA, Groppi VE, Logan SD, and Ashford ML (1997). Leptin inhibits hypothalamic neurons by activation of ATP-sensitive potassium channels. Nature 390, 521–525. [PubMed: 9394003]

Spracklen AJ, Fagan TN, Lovander KE, and Tootle TL (2014). The pros and cons of common actin labeling tools for visualizing actin dynamics during Drosophila oogenesis. Dev Biol 393, 209–226. [PubMed: 24995797]

Teleman AA, Ratzenbock I, and Oldham S (2012). Drosophila: a model for understanding obesity and diabetic complications. Exp Clin Endocrinol Diabetes 120, 184–185. [PubMed: 22402943]

Timper K, and Bruning JC (2017). Hypothalamic circuits regulating appetite and energy homeostasis: pathways to obesity. Dis Model Mech 10, 679–689. [PubMed: 28592656]

Vong L, Ye C, Yang Z, Choi B, Chua S Jr., and Lowell BB (2011). Leptin action on GABAergic neurons prevents obesity and reduces inhibitory tone to POMC neurons. Neuron 71, 142–154. [PubMed: 21745644]

White BH, Osterwalder TP, Yoon KS, Joiner WJ, Whim MD, Kaczmarek LK, and Keshishian H (2001). Targeted attenuation of electrical activity in Drosophila using a genetically modified K(+) channel. Neuron 31, 699–711. [PubMed: 11567611]

Wu Q, Zhao Z, and Shen P (2005). Regulation of aversion to noxious food by Drosophila neuropeptide Y- and insulin-like systems. Nat Neurosci 8, 1350–1355. [PubMed: 16172603]

Xu J, Bartolome CL, Low CS, Yi X, Chien CH, Wang P, and Kong D (2018). Genetic identification of leptin neural circuits in energy and glucose homeostases. Nature 556, 505–509. [PubMed: 29670283]

Yang MJ, Wang F, Wang JH, Wu WN, Hu ZL, Cheng J, Yu DF, Long LH, Fu H, Xie N, et al. (2010). PI3K integrates the effects of insulin and leptin on large-conductance Ca2+-activated K+ channels in neuropeptide Y neurons of the hypothalamic arcuate nucleus. Am J Physiol Endocrinol Metab 298, E193–201. [PubMed: 19671839]

Yoshihara M, and Littleton JT (2002). Synaptotagmin I functions as a calcium sensor to synchronize neurotransmitter release. Neuron 36, 897–908. [PubMed: 12467593]

Zhan YP, Liu L, and Zhu Y (2016). Taotie neurons regulate appetite in Drosophila. Nat Commun 7, 13633. [PubMed: 27924813]

Zhang H, Liu J, Li CR, Momen B, Kohanski RA, and Pick L (2009). Deletion of Drosophila insulin-like peptides causes growth defects and metabolic abnormalities. Proc Natl Acad Sci U S A 106, 19617–19622. [PubMed: 19887630]

Author Manuscript Author Manuscript Author Manuscript Author Manuscript

Zhang YQ, Rodesch CK, and Broadie K (2002). Living synaptic vesicle marker: synaptotagmin-GFP. Genesis 34, 142–145. [PubMed: 12324970]

Author Manuscript Author Manuscript Author Manuscript Author Manuscript

**Highlights:**

- The adipokine leptin/Upd2 reduces inhibitory input to insulin producing cells.
- Arouser, basigin, and gelsolin underpin Upd2-dependent reduction in synapse number.
- Synapse reduction occurs in response to surplus nutrition.
- Insulin resets negative tone by increasing the number of inhibitory contacts.

Author Manuscript Author Manuscript Author Manuscript Author Manuscript

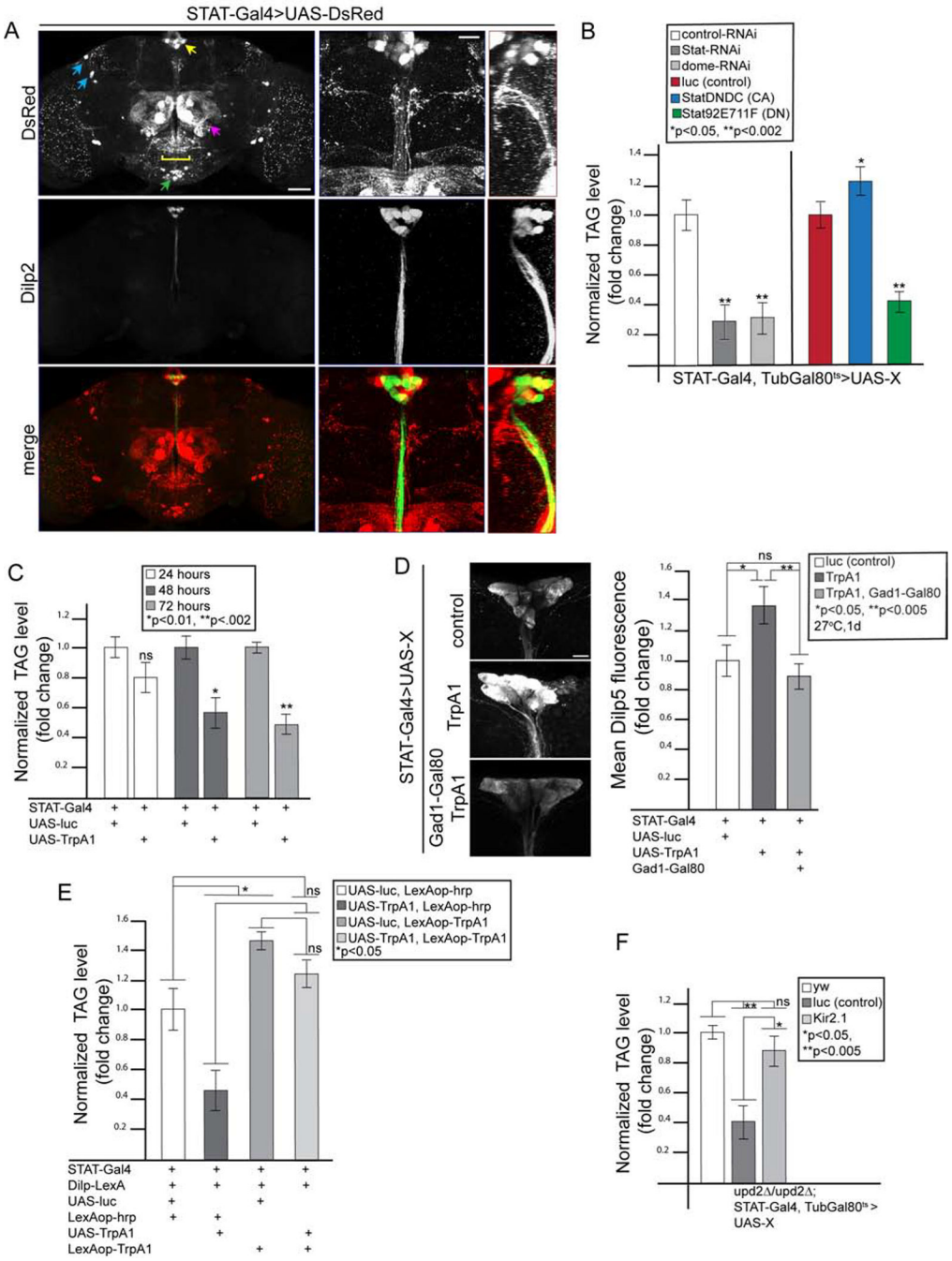


**Figure 1. STAT is expressed in a population of PI GABA neurons that regulate systemic fat storage and Insulin release.**

(A) Analysis of STAT expression in adult brain (STAT-Gal4>UAS-dsRed). Left panels: whole brain view. Yellow arrow indicates PI-STAT somas; yellow bracket, PI-STAT arborizations. Additional expression seen in a bilateral domain (blue arrows), olfactory bulbs (magenta arrow), and SEZ (green arrow). IPCs labeled with α-Dilp2. Middle and right panels in, respectively, the XY and YZ planes, are at higher magnification. Scale bars: 50μm (left panels) and 20μm (middle and right panels). (B, C) TAG analysis of indicated genotypes. (D) Dilp5 immunostaining in IPCs following activation of STAT-expressing

Author Manuscript Author Manuscript Author Manuscript Author Manuscript

neurons with TrpA1, with or without Gad1-Gal80. Quantification of mean Dilp5 fluorescence indicated on the right: n=8 brains per genotype. Scale bar, 10μm. (E, F) TAG analysis of indicated genotypes. Statistical significance calculated by t-test. Error bars represent %SD. For all TAG experiments, 4 replicates of 3 flies each were analyzed.

Author Manuscript Author Manuscript Author Manuscript Author Manuscript

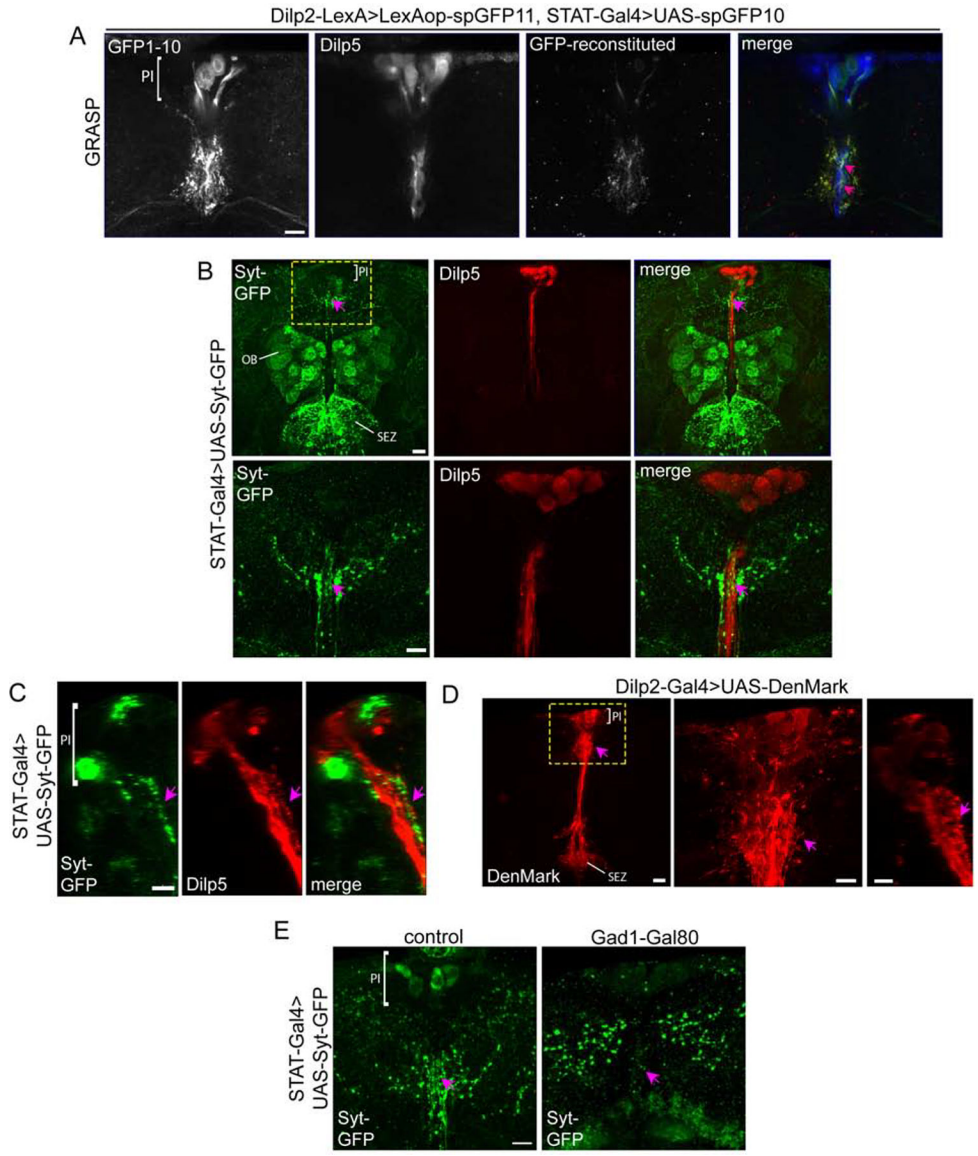


**Figure 2. PI-STAT neurons are in synaptic contact with the IPCs.**

(A) GRASP detection in PI region of adult brain. STAT neurons identified with α-GFP antibody that recognizes spGFP1–10 (first panel); IPCs identified with IHC for Dilp5 (second panel). Points of contact (arrows, merged image) revealed by α-GFP specific to reconstituted GFP (third panel). Scale bar, 10μm. (B) Expression of Syt-GFP via STAT-Gal4 in adult brain at low magnification (upper panels) or high magnification (bottom panels, indicated by yellow dashed rectangle). Arrows point to Dilp5-labelled IPC tracts. Scale bars, 20μm (upper panels) and 10μm (lower panels). (C) Side view of Syt-GFP expression in PI-STAT neurons (YZ plane) showing contact with Dilp5-expressing projections arising from IPC tracts (middle panel). Scale bar, 10μm. (D) Visualization of Dilp2-Gal4 driving expression of UAS-DenMark in IPCs at low (left) or high (middle, XY; right, YZ) magnification. Scale bars, 20μm (left panel) and 10μm (middle and right panels). (E) STAT-

Gal4-driven expression of Syt-GFP in PI-STAT neurons is eliminated by Gad1-Gal80 (arrow). Scale bar, 10μm.

Author Manuscript Author Manuscript Author Manuscript Author Manuscript

Author Manuscript Author Manuscript Author Manuscript Author Manuscript

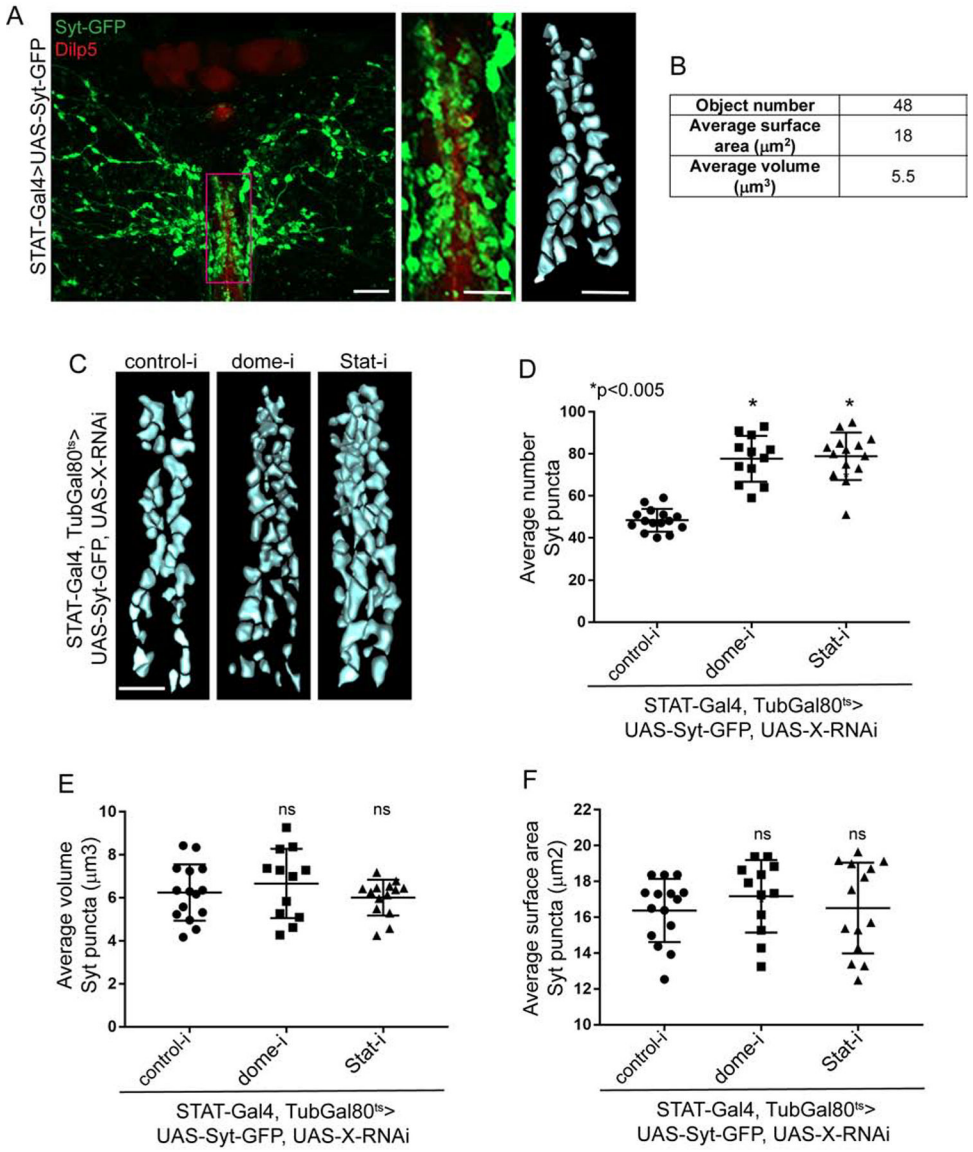


**Figure 3. Assessment of tonic neuronal activity by segmentation analysis of presynaptic bouton number.**

(A) STAT-Gal4-driven expression of Syt-GFP in PI-STAT neurons. IPCs marked by IHC with Dilp5. Box in left panel indicates region of interest seen in middle panel. Right panel shows result of segmentation analysis. Scale bars, 10μm (left) and 5μm (middle and right). (B) Segmentation analysis of PI-STAT neuron boutons in (A). (C) Segmentation analysis of Syt-GFP boutons in PI-STAT neurons of indicated genotypes. Scale bar, 5μm. (D-F) Average number (D), volume (E), and surface area (F) of segmented PI-STAT Syt-GFP boutons following knock-down with indicated RNAi. Each point represents average bouton number, volume, or surface area from a single brain. Between 12–15 brains were analyzed per genotype. For segmentation analysis, statistical significance calculated by 1-way ANOVA on indicated number of individuals. Error bars represent SEM.

Author Manuscript Author Manuscript Author Manuscript Author Manuscript

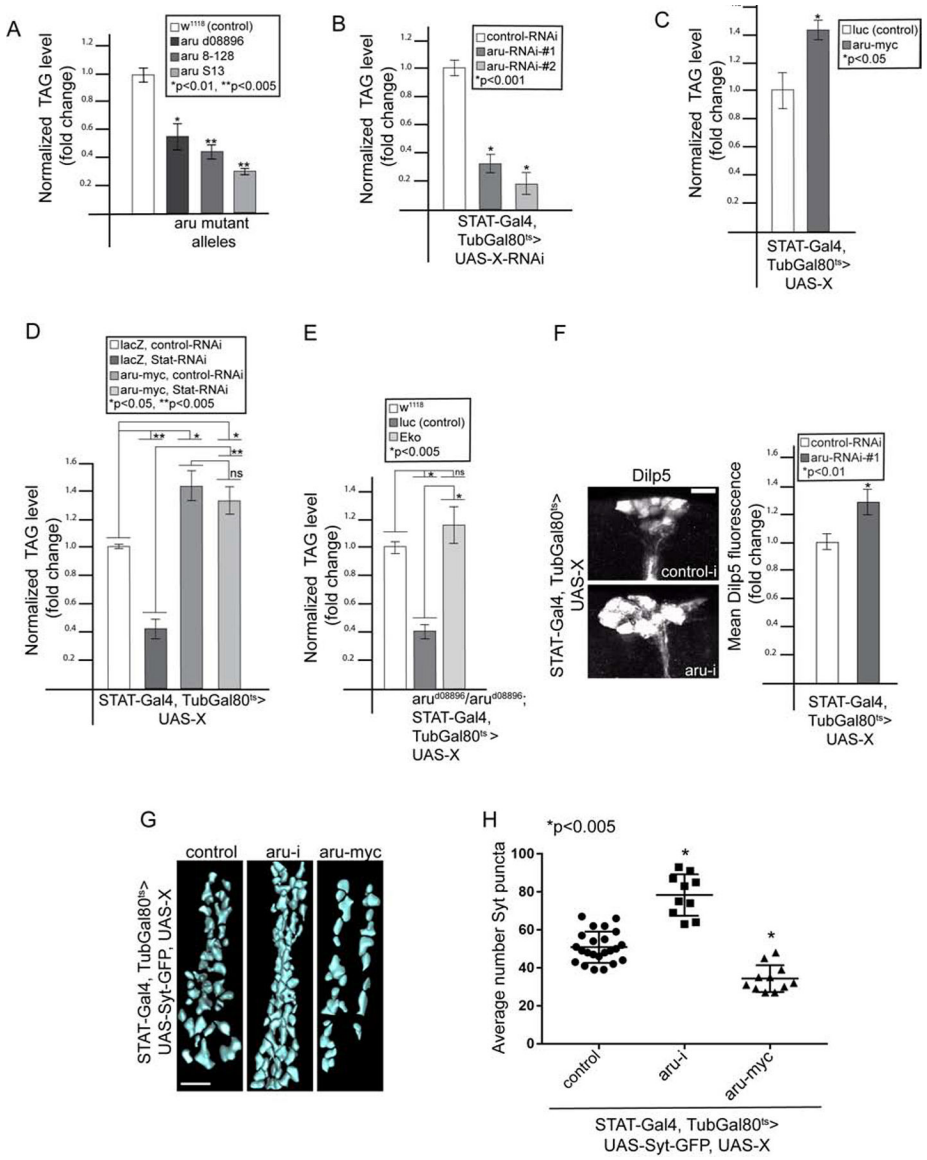


**Figure 4. Arouser functions downstream of STAT to regulate tonic activity in the PI-STAT neurons.**

(A-E) TAG analysis of indicated genotypes. 4 replicates of 3 flies each were analyzed. (F) IHC for Dilp5 in IPCs of adult brains of indicated genotypes. Mean Dilp5 fluorescence quantified on the right: n=15 brains per genotype. Scale bar, 10μm. (G) Segmentation analysis of Syt-GFP boutons in PI-STAT neurons of indicated genotypes. Scale bar, 5μm. (H) Quantification of average number of segmented PI-STAT Syt-GFP boutons in indicated genotypes. Between 10–23 brains analyzed per genotype. For TAG assays and Dilp accumulation, statistical significance calculated by t-test on indicated number of individuals. Error bars represent %SD. For segmentation analysis, statistical significance calculated by 1-way ANOVA on indicated number of individuals. Error bars represent SEM.

Author Manuscript Author Manuscript Author Manuscript Author Manuscript

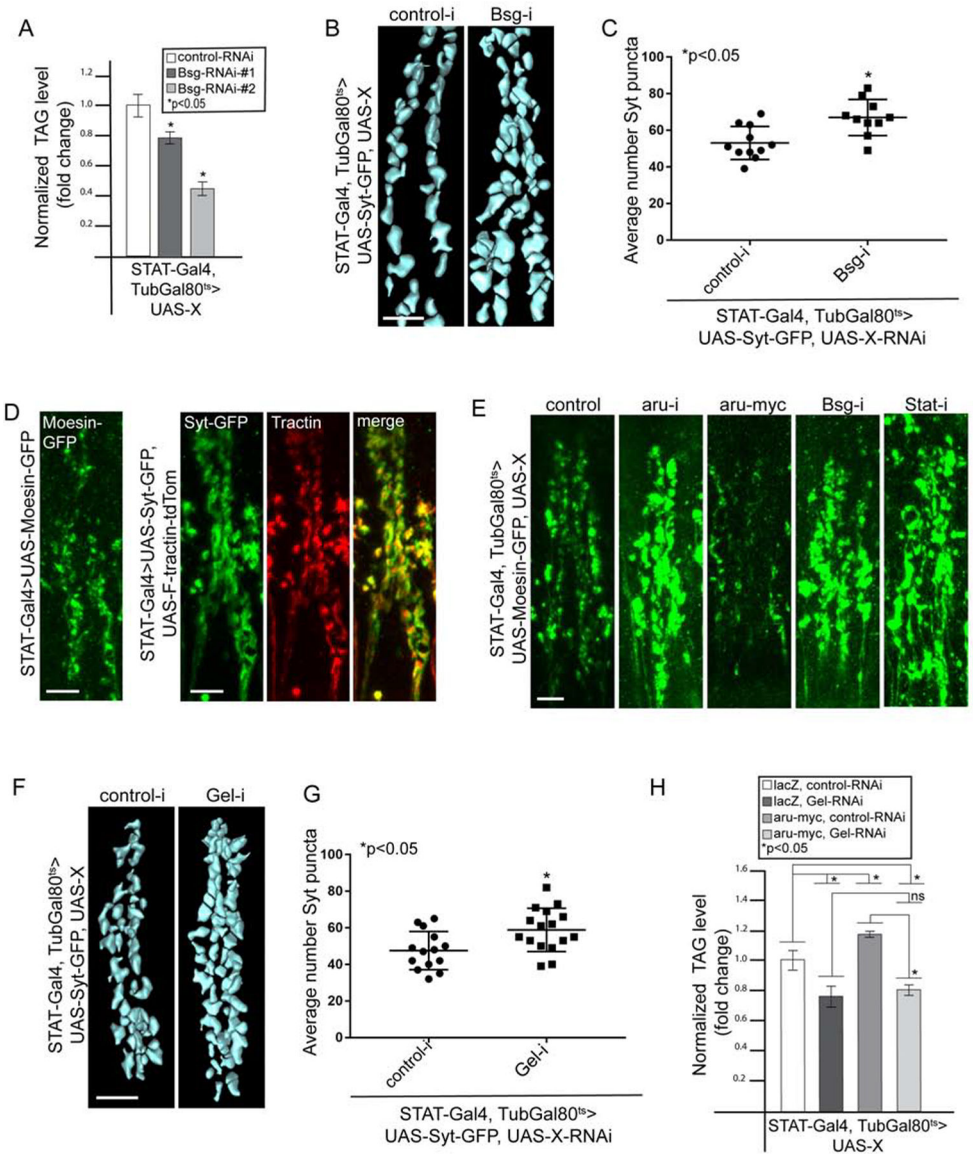


**Figure 5. Aru, Bsg, and Gel regulate PI-STAT neuron bouton number through regulation of the actin cytoskeleton.**

(A) TAG analysis for indicated genotypes; n=4 replicates of 3 flies each. (B) Segmentation analysis of Syt-GFP boutons in PI-STAT neurons of indicated genotypes. Scale bar, 5μm. (C) Quantification of average number of PI-STAT Syt-GFP boutons in indicated genotypes. Between 10–11 brains analyzed per genotype. (D) Left panel, Moesin-GFP expression in PI-STAT neurons, driven by STAT-Gal4. Right panels, expression of Syt-GFP and F-Tractin-tdTom in boutons of PI-STAT neurons, via STAT-Gal4. Scale bar, 5μm. (E) Moesin-GFP expression in adult brain PI-STAT neurons of indicated genotypes. Scale bar, 5μm. (F) Segmentation analysis of Syt-GFP boutons in PI-STAT neurons of indicated genotypes. Scale bar, 5μm. (G) Quantification of average number of PI-STAT Syt-GFP boutons in indicated genotypes. Between 14–16 brains analyzed per genotype. (H) TAG analysis of indicated genotypes; n=4 replicates of 3 flies each. For TAG assays, statistical significance calculated by t-test on indicated number of individuals. Error bars represent %SD. For

segmentation analysis, statistical significance calculated by 1-way ANOVA on indicated number of individuals. Error bars represent SEM.

Author Manuscript Author Manuscript Author Manuscript Author Manuscript

Author Manuscript Author Manuscript Author Manuscript Author Manuscript

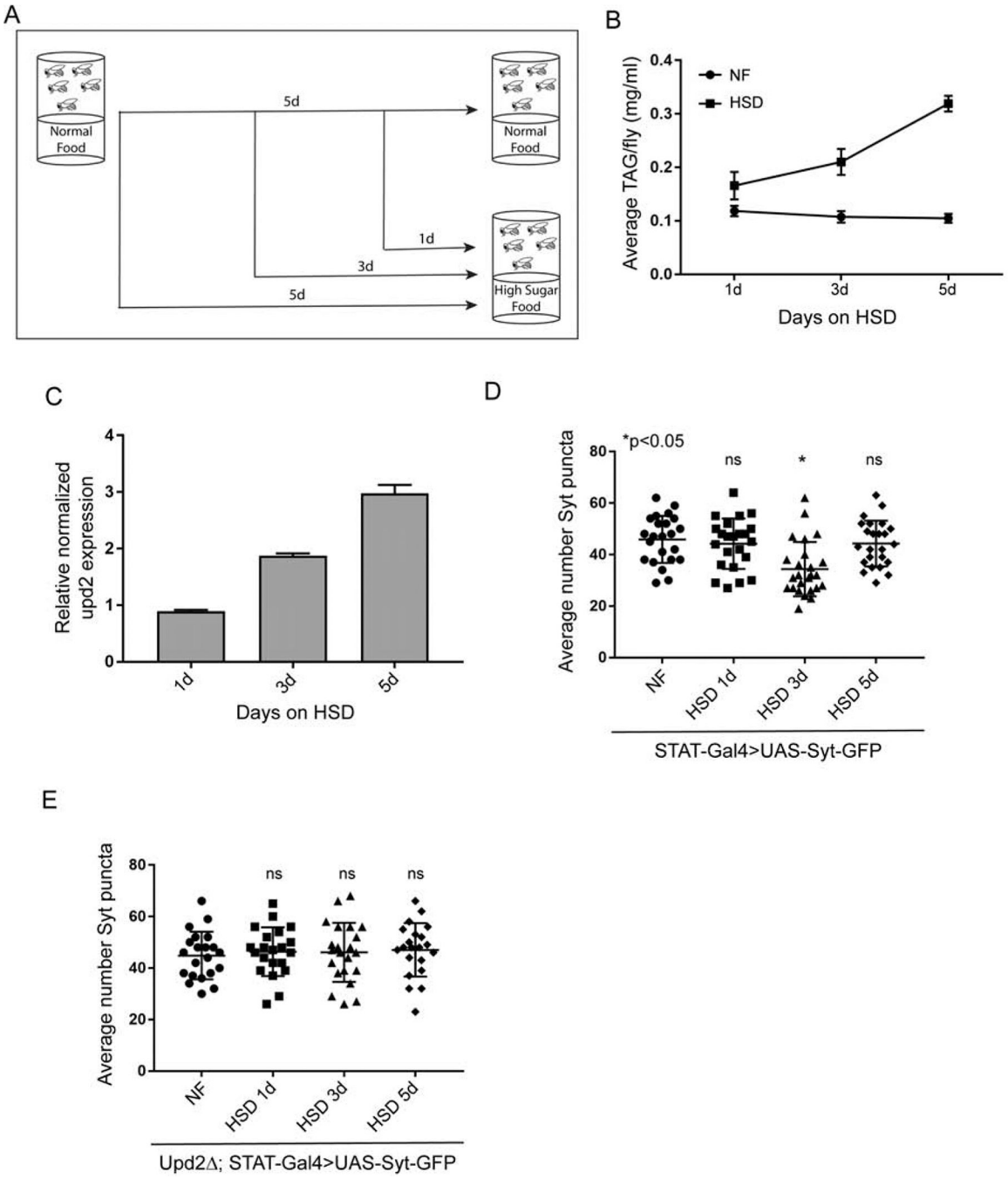


**Figure 6. PI-STAT neuron bouton number adjusts in response to high sugar diet.**

(A) Time-line for HSD exposure. (B) Average TAG/fly in adult flies exposed to NF or HSD (n=4 replicates of 3 flies each). (C) qPCR analysis of normalized *upd2* transcripts in adult flies exposed to NF or HSD. (D, E) Average number of Syt-GFP boutons in PI-STAT neurons of flies exposed to NF or HSD timepoints in (D) control background and Upd2Δ (E). Between 22–25 brains analyzed per condition. For TAG assays and qPCR, statistical significance calculated by t-test on indicated number of individuals. Error bars represent

%SD. For segmentation analysis, statistical significance calculated by 1-way ANOVA on indicated number of individuals. Error bars represent SEM.

Author Manuscript Author Manuscript Author Manuscript Author Manuscript

Author Manuscript Author Manuscript Author Manuscript Author Manuscript

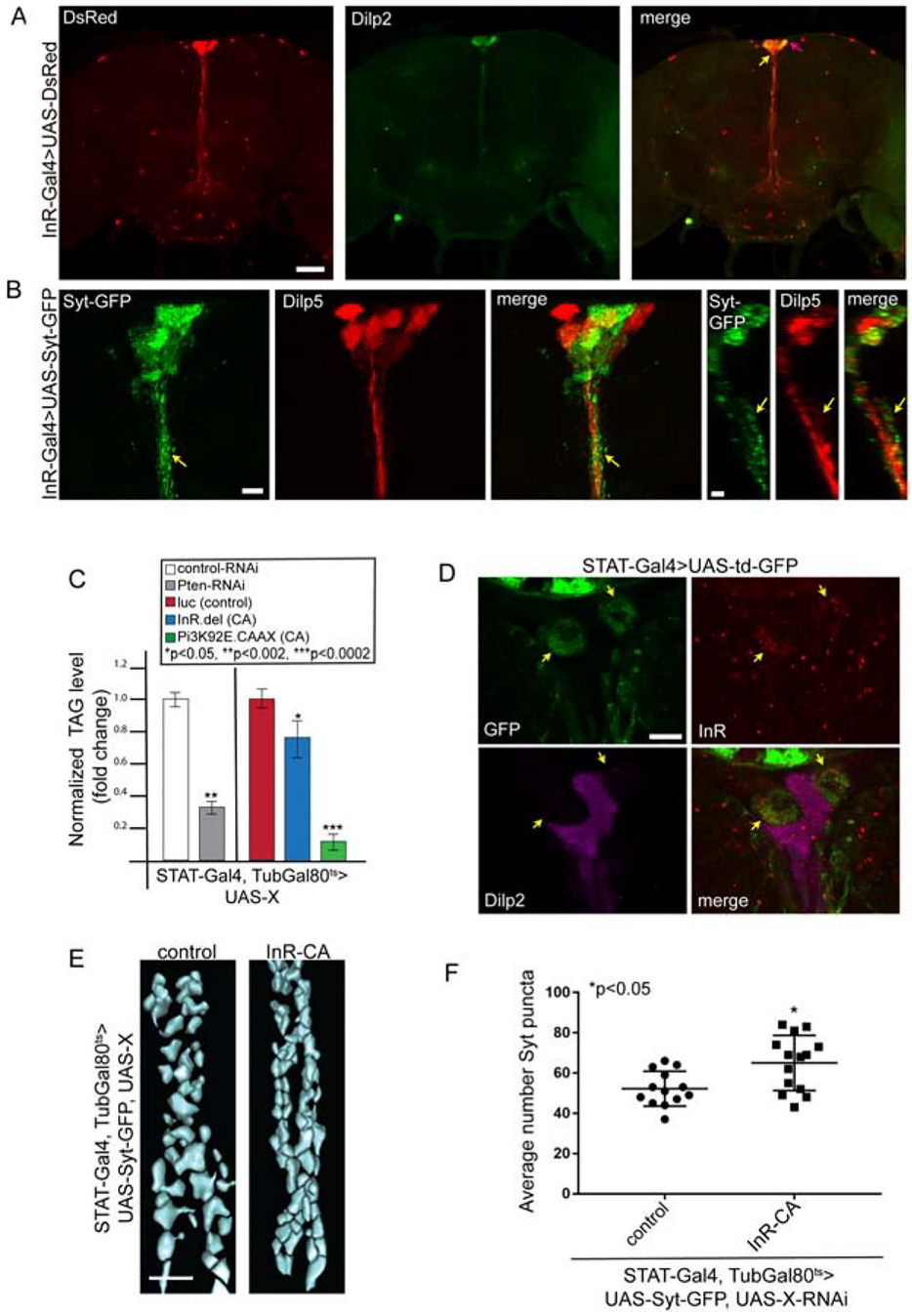


**Figure 7. Insulin signaling promotes inhibitory contacts between PI-STAT neurons and IPCs.**

(A) InR-Gal4-driven expression of dsRed marks population of InR-expressing neurons in PI region. IPCs marked by IHC for Dilp2 (pink arrow: Dilp2-expressing neurons; yellow arrow: non-Dilp2-expressing neurons. Scale bar, 50 μm. (B) Syt-GFP in InR-expressing PI neurons (arrows) (InR-Gal4>UAS-Syt-GFP). First three panels are XY plane, last three are YZ plane. Scale bars, 10μm (XY views) and 5μm (YZ view). (C) TAG analysis performed on indicated genotypes; n=4 replicates of 3 flies each. (D) IHC for InR in td-GFP-expressing PI-STAT neurons (arrows). IPCs labelled via IHC for Dilp2. Scale bar, 10μm. (E)

Author Manuscript Author Manuscript Author Manuscript Author Manuscript

Segmentation analysis of Syt-GFP boutons in PI-STAT neurons of indicated genotypes. Scale bar, 5μm. (F) Quantification of average number of PI-STAT Syt-GFP puncta in (E). Between 13–14 brains analyzed per genotype. For TAG assays, statistical significance calculated by t-test on indicated number of individuals. Error bars represent %SD. For segmentation analysis, statistical significance calculated by 1-way ANOVA on indicated number of individuals. Error bars represent SEM.

Author Manuscript Author Manuscript Author Manuscript Author Manuscript

## KEY RESOURCES TABLE

| REAGENT or RESOURCE | SOURCE | IDENTIFIER |
|---|---|---|
| Antibodies | | |
| Anti-Dilp2 (chicken) | This study | N/A |
| Anti-Dilp5 (rabbit) | This study | N/A |
| Anti-GFP (mouse) | Sigma-Aldrich | Cat# G6539, RRID:AB_259941 |
| Anti-GFP (chicken) | Abcam | Cat# ab13970, RRID:AB_300798 |
| Anti-RFP (rabbit) | Rockland | Cat# 600-401-379, RRID: AB_2209751 |
| Anti-phospho-InR β (Tyr1146) (rabbit) | Cell Signaling Technology | Cat# 3021, RRID: AB_331578 |
| Anti-Brp | DSHB | Cat# nc82, RRID: AB_2314866 |
| Goat anti-Rabbit IgG (H+L) Secondary Antibody, Alexa Fluor 568 | Thermo Fisher Scientific | Cat# A-11036, RRID: AB_10563566 |
| Donkey anti-Chicken IgY (IgG) (H+L) Secondary Antibody, Alexa Fluor 488 | Jackson ImmunoResearch Labs | Cat# 703-545-155, RRID: AB_2340375 |
| Donkey anti-Mouse IgG (H+L) Secondary Antibody, Alexa Fluor 488 | Jackson ImmunoResearch Labs | Cat# 715-545-150, RRID: AB_2340846 |
| Donkey anti-Chicken IgY (IgG) (H+L) Secondary Antibody, Alexa Fluor 647 | Jackson ImmunoResearch Labs | Cat# 703-605-155, RRID: AB_2340379 |
| Bacterial and Virus Strains | | |
| NEB® 10-beta Competent *E. coli* | NEB | Cat# C3019H |
| Chemicals, Peptides, and Recombinant Proteins | | |
| SlowFade® Diamond Antifade Mountant | Thermo Fisher Scientific | Cat# S36963 |
| Myc-Trap Magnetic Agarose | Chromotek | Cat# ytma-10 |
| Paraformaldehyde | EMS | Cat# 19208 |
| Bovine Serum Albumin | Sigma-Aldrich | Cat# A3912 |
| Sucrose | Sigma-Aldrich | Cat# S0389 |
| Fetal Bovine Serum | Thermo Fisher Scientific | Cat# 10437028 |
| Gibco™Penicillin-Streptomycin (5,000 U/mL) | Thermo Fisher Scientific | Cat# 15070063 |
| Gibco™Schneider's *Drosophila* Medium | Thermo Fisher Scientific | Cat# 21720024 |
| Critical Commercial Assays | | |
| iScript™ cDNA Synthesis Kit | Bio-Rad | Cat# 1708891 |
| iQ™ SYBR® Green Supermix | Bio-Rad | Cat# 1708882 |
| Gateway™ LR Clonase™ II Enzyme mix | Invitrogen | Cat# 11791020 |
| Gateway™ BP Clonase™ II Enzyme mix | Invitrogen | Cat# 11789100 |
| Effectene Transfection Reagent | Qiagen | Cat# 301425 |
| Free Glycerol Reagent | Sigma-Aldrich | Cat# F6428 |
| Triglyceride Reagent | Sigma-Aldrich | Cat# T2449 |
| Glycerol Standard | Sigma-Aldrich | Cat# G7793 |
| Direct-zol RNA Miniprep Plus | Zymo Research | Cat# R2071 |
| Experimental Models: Cell Lines | | |
| D. melanogaster cell line S2R+ | Laboratory of Norbert Perrimon | N/A |

Author Manuscript Author Manuscript Author Manuscript Author Manuscript

| REAGENT or RESOURCE | SOURCE | IDENTIFIER |
|---|---|---|
| Experimental Models: Organisms/Strains | | |
| upd2$^{\Delta 3-62}$ | (Hombria et al., 2005) | N/A |
| w$^{1118}$ | N/A | N/A |
| aru$^{08696}$ | (Eddison et al., 2011) | N/A |
| aru$^{8-128}$ | (Eddison et al., 2011) | N/A |
| aru$^{S13}$ | (Eddison et al., 2011) | N/A |
| UAS-Luciferase | TRiP; used in (Rajan and Perrimon, 2012) | N/A |
| UAS-dsRed2 | BDSC | Cat# 8546, RRID: BDSC_8546 |
| UAS-DenMark | BDSC | Cat# 33061, RRID: BDSC_33061 |
| UAS-TrpA1 | BDSC | Cat# 26263, RRID: BDSC_26263 |
| UAS-EKO | BDSC | Cat# 40974, RRID: BDSC_40974 |
| UAS-tdGFP | BDSC | Cat# 35839, RRID: BDSC_35839 |
| UAS-Syt-GFP | BDSC | Cat# 6925, RRID: BDSC_6925 |
| UAS-Moesin-GFP | BDSC | Cat# 31775, RRID: BDSC_31775 |
| UAS-F-Tractin-tdTomato | BDSC | Cat# 58989, RRID: BDSC_58989 |
| UAS-InR-CA | BDSC, Exelexis | Cat# 8254, RRID: BDSC_8254 |
| UAS-PI3K-CA | BDSC | Cat# 8294, RRID: BDSC_8294 |
| LexAop-Hrp | BDSC | Cat# 56523, RRID: BDSC_56523 |
| UAS-Kir2.1 | (Baines et al., 2001) | N/A |
| LexAop-TrpA1 | Provided by Barret D. Pfeiffer | N/A |
| UAS-Synaptophysin-pHTomato | (Pech et al., 2015) | N/A |
| UAS-spGFP1–10 | (Gordon and Scott, 2009) | N/A |
| LexAop-spGFP11 | (Gordon and Scott, 2009) | N/A |
| UAS-STAT92E$^{\Delta N \Delta C}$ | (Ekas et al., 2010) | N/A |
| UAS-STAT92E$^{Y711F}$ | (Ekas et al., 2010) | N/A |
| Gad1-Gal80 | Provided by Toshihiro Kitamoto | N/A |
| UAS-aru-myc | This study | N/A |
| STAT-Gal4 | BDSC | Cat# 62634, RRID: BDSC_62634 |
| Dilp2-Gal4 | (Wu et al., 2005a) | N/A |
| InR-Gal4 | BDSC | Cat# 63762, RRID: BDSC_63762 |
| Dilp2-LexA | This study | N/A |
| luciferase-RNAi | BDSC | Cat# 31603, RRID: BDSC_31603 |
| STAT92E-RNAi | BDSC | Cat# 31317, RRID: BDSC_31317 |
| dome-RNAi | BDSC | Cat# 31245, RRID: BDSC_31245 |
| endoA-RNAi | BDSC | Cat# 27679, RRID: BDSC_27679 |
| cn-RNAi | VDRC | Cat# 105854, RRID: FlyBase_FBst0477680 |
| aru-RNAi-#1 | VDRC | Cat# 105755, RRID: FlyBase_FBst0477581 |

Author Manuscript Author Manuscript Author Manuscript Author Manuscript

| REAGENT or RESOURCE | SOURCE | IDENTIFIER |
|---|---|---|
| aru-RNAi-#2 | NIG | Cat# 4276R-1 , RRID: FlyBase_FBal0274167 |
| Bsg-RNAi-#1 | VDRC | Cat# 43306, RRID: FlyBase_FBst0465019 |
| Bsg-RNAi-#2 | BDSC | Cat# 52110, RRID: BDSC_52110 |
| Pten-RNAi | BDSC | Cat# 25697, RRID: BDSC_25697 |
| Gel-RNAi | BDSC | Cat# 31205, RRID: BDSC_31205 |
| Oligonucleotides | | |
| Primers for mRNA expression | See Table S4 | N/A |
| CACCGCGTGCAACTCGACAATC | This study | Forward primer for Dilp2-LexA |
| AGGTTGCTTTACGATCAAATG | This study | Reverse primer for Dilp2-LexA |
| Recombinant DNA | | |
| Dilp2-LexA | This study | N/A |
| UAS-aru-myc | This study | N/A |
| Software and Algorithms | | |
| AIVIA | DRVISION | N/A |
| GraphPad Prism 7.3 | GraphPad Software | RRID:SCR_002798 |
| CFX Manager 3.1 | Bio-Rad | RRID:SCR_017251 |
| SoftMax Pro Software | Molecular Devices | RRID:SCR_014240 |
| Proteome Discoverer v2.2 | Thermo Fisher Scientific | RRID:SCR_014477 |
| Image J/Fiji | Fiji | RRID: SCR_002285 |
| Zen 2.3 lite | Zeiss | RRID:SCR_013672 |
| Other | | |
| Zeiss LSM 800 | Zeiss | RRID:SCR_015963 |
| SpectraMax i3X | Molecular Devices | N/A |